Root causes analysis of pitting corrosion in copper heat exchangers used in gas water heaters

Ana Paula Sousa Cruz
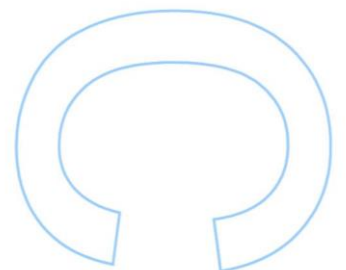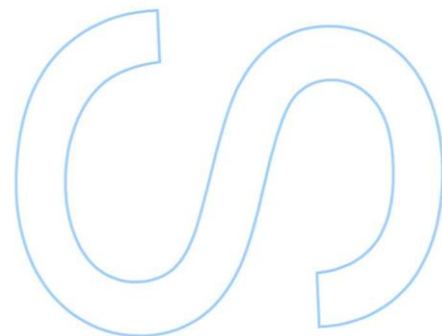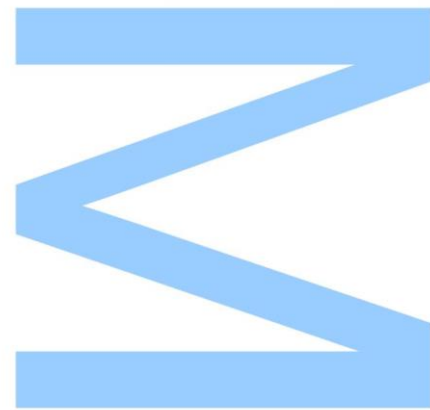
Engineering Physics
Department of Physics and Astronomy
2022

Supervisor
Prof. Dr. Fernando Jorge Monteiro, Full Professor, Faculty of Engineering of the University of Porto

Co-supervisor
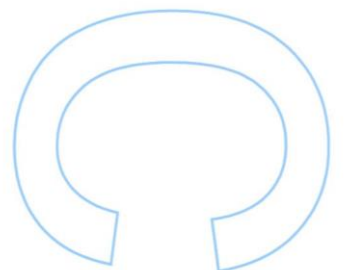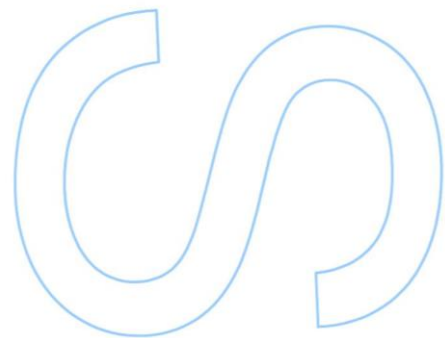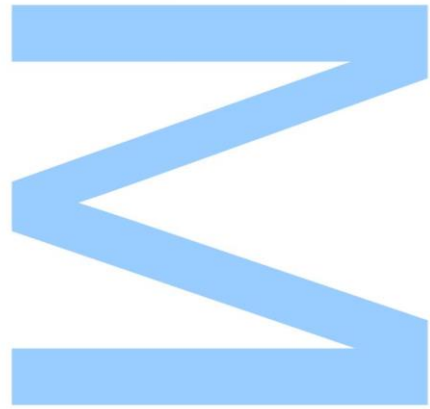Eng. Daniel Alfredo Mota, Senior Manager, Bosch Thermotechnology, S.A – Aveiro

U.PORTO

FC **FACULDADE DE CIÊNCIAS**
UNIVERSIDADE DO PORTO

Todas as correções determinadas pelo júri, e só essas, foram efetuadas.

O Presidente do Júri,

Porto, _____/_____/_____

Sworn Statement

I, Ana Paula Sousa Cruz, enrolled in the master's degree of Engineering Physics at the Faculty of Sciences of the University of Porto hereby declare, in accordance with the provisions of paragraph a) of Article 14 of the Code of Ethical Conduct of the University of Porto, that the content of this work reflects perspectives, research work and my own interpretations at the time of its submission.

By submitting this work, I also declare that it contains the results of my own research work and contributions that have not been previously submitted to this or any other institution.

I further declare that all references to other authors fully comply with the rules of attribution and are referenced in the text by citation and identified in the bibliographic references section. This work does not include any content whose reproduction is protected by copyright laws.

I am aware that the practice of plagiarism and self-plagiarism constitute a form of academic offense.

Ana Paula Sousa Cruz

December 8, 2022

UNIVERSIDADE DO PORTO

ROOT CAUSES ANALYSIS OF PITTING CORROSION IN COPPER HEAT
EXCHANGERS USED IN GAS WATER HEATERS

Root causes analysis of pitting corrosion in copper heat exchangers used in gas water heaters

Author:

Ana CRUZ

Supervisor:

Fernando MONTEIRO

Co-supervisor:

Daniel MOTA

A thesis submitted in fulfilment of the requirements

for the degree of MSc. Engineering Physics

at the

Faculdade de Ciências da Universidade do Porto

Departamento de Física e Astronomia

January 10, 2023

Acknowledgements

To all my colleagues that made these 5 years very special, especially to José Rainha, José Guedes, Filipa Ribeiro and Ana Rita Diogo, thank you so much to all moments and memories.

UNIVERSIDADE DO PORTO

Abstract

Faculdade de Ciências da Universidade do Porto

Departamento de Física e Astronomia

MSc. Engineering Physics

Root causes analysis of pitting corrosion in copper heat exchangers used in gas water heaters

by Ana CRUZ

The main goal of this work is to study the root causes of pitting corrosion in copper heat exchangers used in gas water heaters. For this purpose, all stages of the manufacturing process of copper heat exchangers were followed and was outlined an experimental plan with three distinct phases to test the most crucial stages of the manufacturing process. In the first phase, the corrosion products present in the heat exchangers were evaluated using XRD and SEM/EDS. In the second phase, copper samples with different provenances were metallographically characterized and tested through potentiodynamic polarization and electrochemical impedance spectroscopy. In the third phase, were analysed parameters of water used in the functional tests.

With XRD analysis was verified the presence of malachite outside of the heat exchanger and the presence of chlorine and sulfur inside the copper coils in the region of pits. Based on the potentiodynamic polarization technique It was observed the occurrence of pitting corrosion in a solution of 0.1M of sodium sulphate for the different samples. The presence of carbon was verified in the region of pits in the sample with Lubsec oil used in the manufacturing process of heat exchangers. After analysing the water used in the functional tests, it was found that the chlorine level was considerably high.

In summary, was possible to identify root causes with this work and make suggestions at the level of the manufacturing process of the heat exchangers. It was suggested to wash the pipes to remove the residues of the lubsec oil and the improvement of water used in the functional tests.

UNIVERSIDADE DO PORTO

Resumo

Faculdade de Ciências da Universidade do Porto

Departamento de Física e Astronomia

Mestrado em Engenharia Física

Análise das causas raiz da corrosão por picada em câmaras de combustão de cobre usadas em esquentadores a gás

by Ana CRUZ

Este trabalho tem como principal objetivo o estudo de causas raiz da corrosão por picada em câmaras de combustão de cobre usadas em esquentadores a gás.

Para tal, acompanhou-se todas as etapas do processo de fabrico das câmaras de combustão de cobre e delineou-se um plano experimental de modo a testar as etapas mais fulcrais do processo. Numa primeira fase avaliou-se os produtos de corrosão presentes na câmara de combustão e usou-se XRD e SEM/EDS como técnicas de análise. Na segunda parte do trabalho experimental caracterizou-se metalograficamente amostras de cobre com diferentes proveniências que posteriormente foram testadas com téncicas de polarização potenciodinâmica e espetroscopia de impedância eletroquímica.

Com a análise XRD verificou-se a presença de malachite no exterior da câmara de combustão e verificou-se a presença de cloro e enxofre no interior da câmara na zona das picadas. Com base das técnicas de polarização potenciodinâmica verificou-se a ocorrência de picadas numa solução de 0.1M de Sulfato de Sódio para as diferentes amostras, tendo-se associado a presença de carbono à inicação de picadas na amostra com óleo Lubsec usado no processo de fabrico das câmaras de combustão. Após a análise da água usada nos testes funcionais verificou-se que o nivel de cloro é consideravelmente elevado.

Em suma, de modo a identificar causas raiz com o trabalho elaborado foi possivel elaborar sugestões a nivel de processo de produtivo das câmaras, que passam pela lavagem dos tubos e melhoria da água usada nos testes funcionais.

Contents

List of Figures

List of Tables

Glossary

NACE	National Association of Corrosion Engineers
GDP	Gross Domestic Product
SA	Sociedade Anónima
TT	Thermotechnology
EPM	Engineering Product Quality, Processes and Methods
CE	Center of Engineering
ISO	International Standards Organization
EN	European Norm
pH	potential of hydrogen
AC	Alternating current
XRD	X-ray diffraction
SEM	Scanning Electron Microscopy
EDS	Energy Dispersive Spectroscopy
SE	Secondary Electrons
BSE	Backscattered Electrons
FEG	Field Emission Gun
CCD	Charged Coupled Device
ABS	Acrylonitrile Butadiene Styrene
ASTM	American Society for Testing and Materials
DHP	Deoxidized High Phosphorus
CFD	Computational fluid dynamics

Chapter 1

Introduction

This chapter presents the problem definition, goals to be achieved, followed by methodology and presentation of the business unit where the project was carried out.

1.1 Problem Definition

Corrosion is a costly problem in our industrialized society, affecting a large number of sectors. Since the industrial revolution in the late eighteenth century and with technological progress, corrosion costs are higher and prevention is becoming an important factor at the industrial level to avoid or minimize future corrosion processes. A study performed in the United States carried out by NACE estimates that annual costs of corrosion reached 2.5 trillion € per year, which is equivalent to 3.4 % of the GDP (2013) [1]. Pitting corrosion is a type of localized corrosion and represents a wide range of corrosion problems in today´s industrial sector. Many variables are involved in this phenomenon, almost every feature of a metal/environment system has an effect on pitting corrosion. Although considerable knowledge has been acquired over the past decades, pitting remains and is considered by several authors a major issue in corrosion science [2–4].

This work aims to investigate possible root causes for the occurrence of pitting corrosion in copper heat exchangers used in gas water heaters produced at Bosch Thermotechnology, S.A - Aveiro. The largest number of failures (78%) occurs in the cold water coil of heat exchangers as illustrated by figure 1.1. The first occurrence of pitting corrosion at Bosch in heat exchangers occurred in 2003. The field failures reported occurred mostly in Italy, Germany, Poland, Spain and Portugal.

FIGURE 1.1: Illustration of the coil of the heat exchanger where 78% of the failures occur.

In 2021, Bosch Thermotechnology, S.A - Aveiro estimated the annual cost due to pitting corrosion in heat exchangers to be around 140.000€/year, considering direct and indirect costs including labor, replacement of equipment and logistics costs. Over the years, various containment measures were taken, such as implementing carbon-free raw material in accordance with the EN1057 standard and increasing the thickness of the copper used in heat exchangers (from 0.60 to 0.71mm).

To study the problem described above and possible root causes, the work was structured in order to follow and analyse the manufacturing process of copper heat exchangers, emphasising the most critical phases. An experimental plan was elaborated in order to give inferences concerning the influence of the the manufacturing process of the heat exchangers, using as experimental techniques XRD, SEM/EDS, metallographic characterization of copper samples from different provenances, potentiodynamic polarization and electrochemical impedance spectroscopy. Based on the experimental results obtained it is intended to provide hints towards improving the current manufacturing process of heat exchangers.

This project was developed at the Business unit Bosch Thermotechnology, S.A - Aveiro, based in Cacia, Aveiro district. This work is integrated in the curricular unit "Internship" of the master's in Engineering Physics of the University of Porto. The internship was carried out during the period from March 14, 2022 to September 14, 2022, specifically in the TT/EPM - CE team.

1.2   Goals

The main goal of the present work was to identify possible root causes of pitting corrosion in copper heat exchangers used in gas water heaters and present possible solutions. With this aim, pits were analysed and information was collected from the manufacturing process, understanding the production process and possible causes for the failure. The project selection was carried out by Bosch Thermotechnology, S.A - Aveiro due to the considerable number of failures in recent years and the high costs for the company with this failure mechanism. Pitting Corrosion in copper heat exchangers has a high number of variables involved, making this problem very complex. Considering that chemical composition of the water circulating in the water heaters cannot be changed/corrosion inhibitors cannot be added, the main goals of this work were:

- Analysis of the manufacturing process of heat exchangers to identify possible root causes, including: skirt manufacturing, coils manufacturing, elbows and U-pipes manufacturing, furnace brazing, dry test and functional test;

- Analysis of pits using XRD and SEM/EDS;

- Experimental delineation to investigate and check possible causes, through the definition of the relevant experimental methods, namely: metallographic characterization, potentiodynamic polarization and electrochemical impedance spectroscopy.

- Proposal of improvements in the manufacturing process to reduce the probability of failures.

1.3 Methodology

The present work is divided into seven chapters. The first chapter presents the framework of the project, goals, methodology and business unit. It transmits information about the history of the company, structure, products manufactured and basic working principle of a gas water heater.

The second chapter presents the bibliographic survey, being the main focus to address the mechanism, classification, respective causes and electrochemical methods described in the literature for pitting corrosion in copper.

The third chapter presents the manufacturing process of heat exchangers. It transmits information about the key stages of the manufacturing process of heat exchangers that may have an influence on the problem being studied, the most critical points are summarized in a fault tree analysis.

The fourth chapter presents the materials and methods used in the experimental work of this project, namely: XRD, SEM/ EDS, metallographic preparation, potentiodynamic polarization and electrochemical impedance spectroscopy.

The fifth chapter concerns the results and their discussion, in this chapter the results obtained in the experimental section are presented and discussed.

Finally, the seventh chapter presents the main conclusions of the work developed and makes suggestions for future improvement actions.

1.4   BOSCH Thermotechnology, S.A - Aveiro

This work was developed at Bosch Thermotechnology, S.A - Aveiro, the leading manufacturer of products for sanitary water heating. Bosch Thermotechnology, S.A - Aveiro started in 1977 as Vulcano Termodomésticos, S. A - Aveiro in Cacia, Aveiro district. Today, with more than 1000 employees, the company develops solutions for domestic and heating purposes. Originally, this company consisted exclusively of the national capital and was dedicated to the manufacture and sales of gas water heaters in Portugal. The growth based on the quality of the manufactured appliances and a well-organized sales strategy, consolidated in 1983 with the introduction of its own brand, Vulcano, and after-sales service, guarantee the company a fast and solid leadership in the national market of water heaters.

In 1988, with the acquisition of the majority of the capital by the group Bosch, the Vulcano plant, now Vulcano Termodomésticos, S.A., becomes part of the Bosch Termotecnologia Division, transferring the existing competencies and equipment to Portugal, starting a specialization process within the group.

In 1992, Vulcano Termodomésticos, S.A., reached the leadership of the European market and the 3rd place in the production of water heaters worldwide. With these excellent results, the company becomes Robert Bosch's competence center for this product, thus being responsible for the design and development of new products as well for manufacturing and commercialization.

Currently, the products manufactured at the Business unit located in Aveiro are Gas and Electric Water Heaters (1.1 million units/year), Boilers (84 k units/year) and Heat Pumps (4 k units/year). Given that the focus of this work is to study pitting corrosion in copper heat exchangers used in gas water heaters, the working principle and structural division are described in the following subchapter.

1.4.1   Working principle of a gas water heater

A gas water heater is an appliance powered by gas intended to perform the instantaneous heating of sanitary water. The common and usual structural composition of a gas water heater is divided into four large groups as shown in the following figure: (1) gas/water valve, (2) safety sensors, (3) heat exchanger and (4) draught diverter.
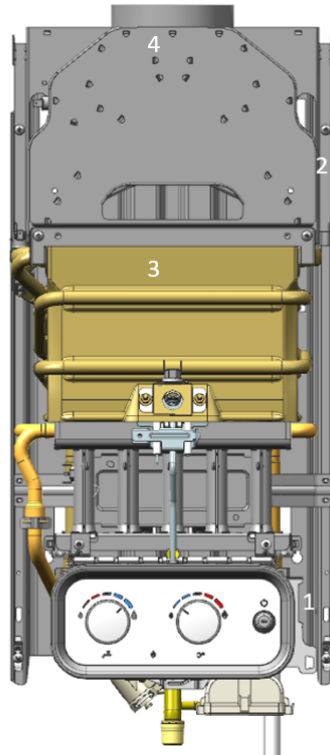
FIGURE 1.2: Strutural composition of a gas water heater.

The function of gas/water valve is recognizing "the need of hot water", in other words, when a hot water tap is opened a flow of water is generated inside the automatic water that moves a piston that is later connected to the gas automatic. Gas valves are made up of two solenoid valves: pilot valve and membrane valve. The pilot valve controls the admission of gas to the injection pilot and the membrane valve is responsible for controlling the passage of gas to the injectors.

The water heater also has several safety devices, which ensure that the water heater does not endanger its user. The group of safety sensors consists of a ionization probe, microswitch, temperature sensors and detection sensors of combustion product. The ionization probe detects the presence of the pilot burner flame and signals the electronic control unit to turn the gas supply on or off to ignite the main burner. The microswitch

corresponds to a small "electric switch" placed next to the automatic water, whose main function is to send a signal to the control unit indicating whether water flow is present in the water heater. The temperature sensor blocks the water heater when the water temperature exceeds a previously defined value (85ºC), typically placed at the outlet of the pipe. NTC (Negative Temperature Coefficient) devices are usually used, which are resistors that vary with temperature. The detection sensor of combustion products is located in the area of the deflectors and has the main function of detecting possible blockages in the draught diverter.

The heat exchanger represented by point 3 is responsible for heating the water in the circuit and is composed by the following components: skirt, cold water coil, hot water coil, U pipes and Fins. The skirt has a rectangular geometry and is helically wrapped by a cold water coil and a hot water coil. The helical shape of the pipes aims to cool the walls of the heat exchanger (skirt) avoiding phenomena such as thermal fatigue. In the upper region of the heat exchanger is the region where the most of heat energy is transferred from the burned gases to water.

Finally, it is important to consider 3 fundamental characteristics for the characterization of a gas water heater, namely: capacity, type of gas and exhaustion of combustion products.

1. The capacity represents the amount of hot water in liters per minute that the appliance working at maximum power can raise a temperature of 25ºC between the inlet and outlet water temperature.

2. The type of gas used can be divided into three families based on the Wobbe index (that represents the quotient between the calorific value and the square root of the relative density of the air index) namely: 1st family (city gas), 2nd family (natural gas) or 3rd family (Liquefied petroleum gas (LPG)).

3. Exhaustion of combustion products can be carried out by natural exhaustion: Open Flue (OF) or forced exhaustion: Fan Pressurized (FP). In OF appliances, the flow of combustion products, as well as the admission of air for combustion, takes place through natural convection. On the other hand, the FP has a fan that helps the expulsion of gases through the exhaust duct.

Chapter 2

State of The Art

This chapter presents the literature review conducted, presenting important concepts for this work. First, the main types of corrosion described in the literature are discussed. Then, emphasis is placed on pitting corrosion, namely the theoretical mechanism, classification and the main causes described in the literature are addressed. Finally, the electrochemical methods relevant to this work are presented.

2.1 Corrosion

According to ISO 8044, corrosion is defined as:" Physicochemical interaction between a metal and its environment which results in changes of the metal's properties and which may lead to significant functional impairment of the metal, the environment or the technical system of which they form a part" [5].

Some authors consider corrosion as a phenomenon opposite to metallurgy because while metallurgy corresponds to the gain of energy by the transfer of the compound from the raw material to the metallic material, corrosion corresponds to the loss of energy by the transition of the metallic material to its original state. Iron, for example, occurs naturally in the form of iron oxide, which has a low-energy state. As the iron ore is transformed into metal, the energy level increases (e.g. in a blast furnace), making the metal less stable than the original ore as illustrated in figure 2.1 [6].
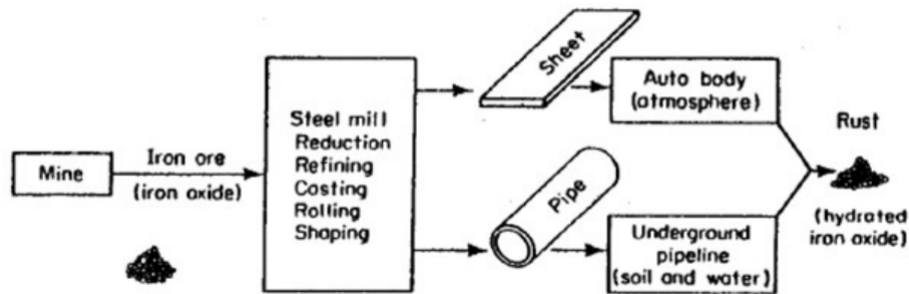
FIGURE 2.1: Mettalurgy in reverse. Adapted from [6].

As all materials in the universe endeavor to return to their lowest energy state, pure metals also strive to revert to their lowest energy state which they had as sulfides or oxides. One of the ways in which metals can revert to a low energy level is by corrosion. Corrosion of metals is considered an electrochemical process involving two half-reactions: oxidation of the metal and reduction of the chemical species receiving electrons from the oxidation. The Gibbs free energy gives information about the spontaneity of the process and is translated by the following equation:

$$\Delta G = -nFE \tag{2.1}$$

In the equation described earlier, ΔG corresponds to the Gibbs free energy, where n is the number of electrons present in the electrochemical reaction, F is the Faraday constant, and E is the potential difference between the species that is reduced and the species to which it is oxided. The reaction is said to be spontaneous if ΔG is negative and ΔE is positive. On the other hand, if ΔG is positive reaction is not spontaneous [7].

According to Fontana, it is possible to classify corrosion according to its appearance and morphology, proposing eight types of corrosion illustrated in figure 2.2. The author proposes the following types: uniform corrosion, galvanic corrosion, pitting corrosion, intergranular corrosion, crevice corrosion, erosion corrosion, selective leaching and stress corrosion cracking [6].
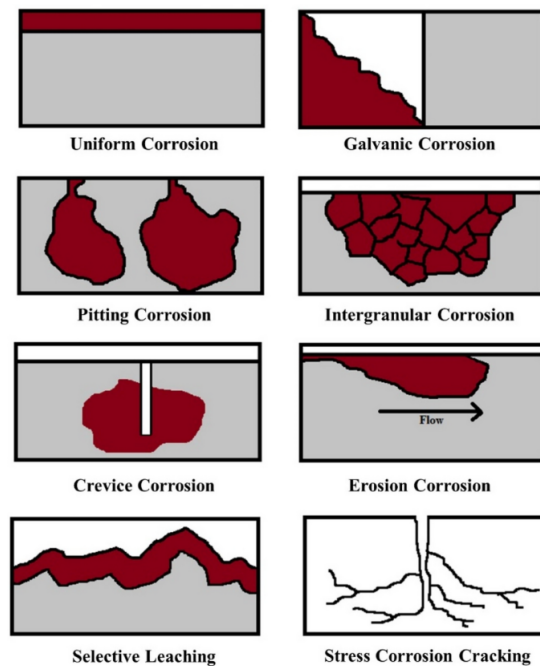
FIGURE 2.2: Different types of corrosion according to Fontana. Adapted from [8].

Uniform corrosion is the most common form of corrosion and is characterized by an attack along the surface at a uniform rate, resulting in the loss of corroded material and consequent reduction in the thickness of the metal. For example, a piece of steel or zinc immersed in sulfuric acid dissolves uniformly over the entire surface [6].

Galvanic corrosion is defined by the electrochemical action resulting from electrical contact between two conductive materials immersed in the same conductive electrolyte. The material whose potential is more positive acts as the cathode and the material with the more negative potential acts as the anode and is preferentially corroded. Cathodic protection results from the application of this principle, a very common example is the use of zinc ingots in iron boats, where the zinc corrodes and the iron is protected.

Pitting corrosion is characterized by being highly localized, with attack regions leading to small holes that can reach the metal and cause perforation of the material. It usually occurs in passive metals in the presence of certain ions, the most common in the literature is Cl^- [6]. Examples of metals subject to pitting corrosion include stainless steel, aluminum and copper alloys. In the next subsection, this type of corrosion will be discussed in more detail.

Intergranular corrosion is characterized by the preferential attack at grain boundaries. One of the most common cases of intergranular corrosion occurs in stainless steels, since there is a difference in chemical composition of material due to the formation of a chromium-depleted region in the vicinity of the grain boundaries as a result of the precipitation of chromium carbides [9].

Crevice corrosion is considered a type of localized corrosion characterized by the presence of crevices or shielded areas on the metal surface exposed to the corrosive environment. This type of attack is associated with stagnant solutions and small volumes. This type of corrosion occurs due to the difference in oxygen content between two areas of metals, creating an electrochemical cell.

Erosion-corrosion corresponds to the increase of material wear and mechanical abrasion on the metal surface at the same time as the corrosion attack. The most common examples are fretting corrosion and cavitation.

Finally, stress corrosion cracking, as the name implies, is the result of a localized attack or fracture caused by the synergistic action of a mechanical factor and corrosion. The most common forms are stress corrosion cracking, fatigue corrosion and hydrogen embrittlement. The combination of corrosion and mechanical stress is, as the name implies, a localized attack or fracture caused by the synergistic action of a mechanical factor and corrosion.

2.2   Pitting Corrosion

Pitting Corrosion is a form of localized corrosion that leads to the creation of small holes in the material [5]. Pitting Corrosion is widely known as one of the most dangerous types of corrosion because it is difficult to predict and detect (pits are often covered by corrosion products). In addition, it is difficult to measure quantitatively and compare the extent because of the number of depths and number of pits that occur in identical conditions [6]. According to ASTM G46-21 Standard [10], pits can have different morphologies depending on the metallurgy and chemistry of the environment and are sketched in figure 2.3. Pits can be narrow, elliptical, wide, subsurface, undercutting, horizontal or vertical.
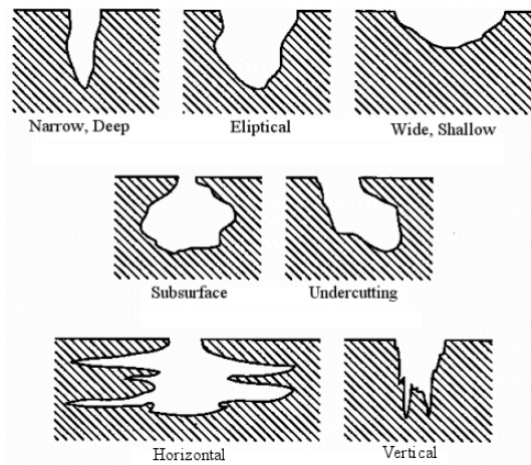
FIGURE 2.3: Variations in cross sectional of pits. Adapted from ASTM G46-21 Standard [10].

Maximum pit depth (D) can be expressed by the following empirical equation:

$$D = kt^{\beta} \qquad (2.2)$$

Where k is a proportionality factor that depends on the material, environment and surface area, t is the exposure time and β is the pitting exponent. Measurement of pit depth is one way to obtain an indicator of mass loss. Pit depth can be measured by a variety of methods, usually involving metallographic preparation and optical microscope measurements [10].

Despite advances in recent years, the fundamental understanding and prediction of localized corrosion is complex for several reasons. It is important to emphasize that initiation events are relatively difficult to predict because they have a stochastic nature [4, 11].

2.2.1 Mechanism

Frankel conducted a comprehensive study about the mechanism of pitting corrosion. In his work, he divided the mechanism into three distinct phases, namely: passive film breakdown, metastable pitting, and pitting growth [12]. According to Frankel, the destruction of the passive film and the initiation of pitting is perhaps the least understood aspect of the pitting phenomenon. The passive film has the ability to cover the underlying metal and block environmental access to it and depending on the material composition, environment and potential this layer can vary in thickness, structure, composition and protection (typically, a passivated layer is very thin).

According to Frankel passive film breakdown and pit initiation have been divided into three main mechanisms. The model proposed by Frankel for passive film degradation includes film penetration, absorption, and film breaking as shown in figure 2.4.
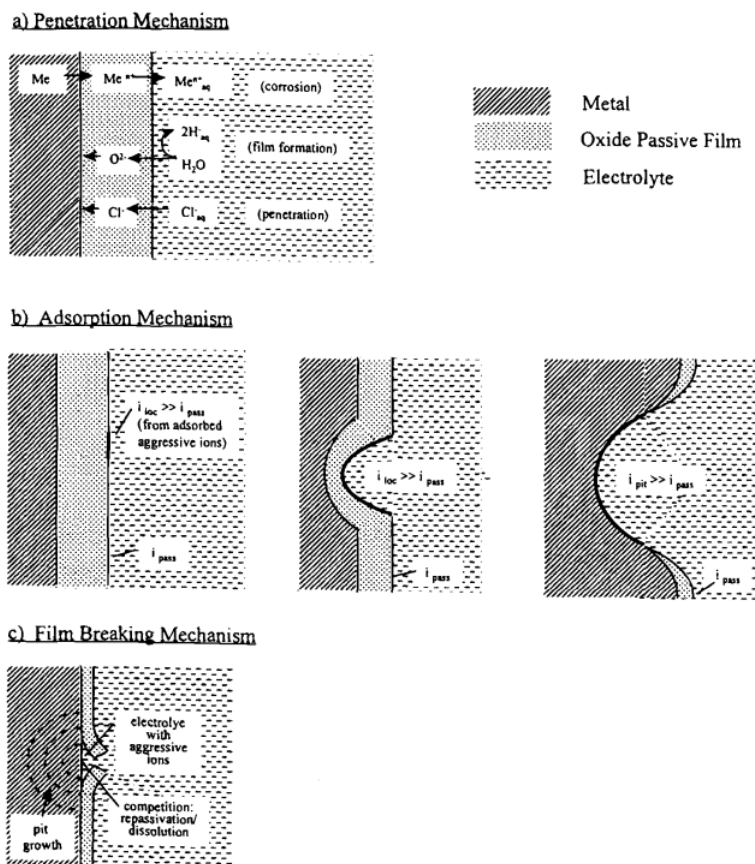
FIGURE 2.4: Schematic of mechanism of passive film breakdown according to Frankel [12].

The second phase corresponds to metastable pitting. Metastable pits are characterized by growing only for a limited time before being reactivated. Large pits can stop growing for a variety of reasons, but metastable pits are usually less than a micrometer in size and have a lifetime on the order of seconds.

The third phase corresponds to pitting growth, which usually depends on the material composition, electrolyte, and potential. Typically the mass transport properties of the pit affect the kinetics of pit growth through the concentration of the pit electrolyte, as described above. Pit stability depends mainly on the composition of electrolyte.

According to Sarver if the material is copper pits can initiate at specific locations, including imperfections or breakdowns in the passive film layer that naturally occurs on copper surfaces in potable water [13]. According to Cong, it is generally accepted that copper forms a duplex layer film in neutral alkaline solutions. The inner layer in contact with pure copper is copper oxide I (Cu_2O) and the outside layer depends mostly on the chemistry of solution (e.g. cupric oxide (CuO), cupric hydroxide ($Cu(OH)_2$)) [14].

After initiation, propagation can be increased by differential concentration cell, due to changes that occur in a small region. According to Sarver, the pit water becomes very acidic due to Lewis acidity of released Cu^{+1} and Cu^{+2} ions, and salty due to the increasing anion (e.g., Cl^- and SO_4^{2-}) concentrations drawn into the pit to maintain electro-neutrality as illustrated by figure 2.5.
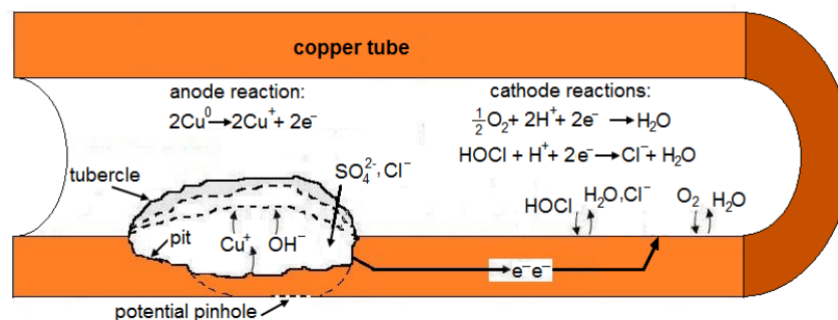
FIGURE 2.5: Simplified depiction of pitting corrosion of a copper tube. Electrons produced at the anode are consumed at the remote cathode. Adapted from [13].

2.2.2 Classification

In the literature, there are three different classifications for copper pitting corrosion, namely: Type I, Type II and Type III [11, 14]. According to Pourbaix Pitting Type I has traditionally been observed in cold water pipes in the presence of carbon films. According to the models presented in the literature Type I contains crystalline cuprous oxide (CuO_2) and copper chloride ($CuCl$) inside pit as illustrated by figure 2.6 [11, 15].
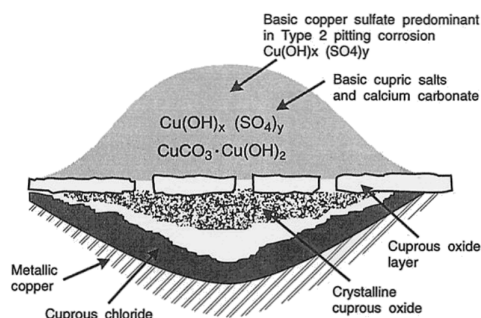
FIGURE 2.6: Pitting corrosion Type I according to Geesey [15].

On the other hand, Pitting Type II has been observed in hot water(with a temperature above 60 °C) and the ratio of bicarbonate sulphate (HCO_3^- / SO_4^{2-}) is <1 [11]. It occurs in countries with predominantly soft water, such as Scandinavia and Japan and failures usually occur after 8 to 12 years of operation. Typically it presents a narrow opening and irregular geometry. The surface of the pits consists mostly of basic copper sulfate [16].

Finally, Pitting Type III also known as "soft water pitting" is associated with low hardness and high alkalinity. Type III has been reported in Sweden and pits presents a wide and shallow geometry [15, 17, 18].

2.2.3 Causes

Several factors are mentioned in the literature that can promote pitting corrosion. If the material is copper, the main causes indicate the synergistic effect of several factors, namely: microstructure, carbon films, soldering flux, pH, chloride, chlorine, sulfate and the presence of microorganisms. Table 2.1 shows an overview of the different causes found in the literature.

TABLE 2.1: Literature Review: Causes for Pitting Corrosion in Copper.

Factor	Causes	References
Material	Microstructure	[19]
Material	Carbon films	[9, 20, 21]
Material	Soldering flux	[22, 23]
Environment	pH	[14, 24]
Environment	Chloride	[24, 25]
Environment	Chlorine	[26]
Environment	Sulfate	[27]
Environment	Microbial activity	[28]
Environment	Water flow	[29]

2.2.3.1 Microstruture

The literature points out that the microstructure plays an important role in the pitting corrosion of copper. Yanhuki and co-workers studied the pitting behavior for different grain sizes, namely 23, 67 and 470 μm, using cyclic polarization and electrochemical impedance spectroscopy. Authors concluded that for a test solution of 0.1 M of sodium sulfate (Na_2SO_4) + 0.1 M of sodium hydroxide (NaOH), a higher grain size (470 μm) leads to the highest susceptibility to pitting corrosion, explaining that the increase in grain size causes more susceptibility through the decrease of quality of the copper passive film formed [19].

2.2.3.2 Carbon films

The presence of carbon films has also been cited in the literature and associated with pitting corrosion in copper. One of the first authors to address the above topic was Campbell in the year of 1950. The work developed by Campbell shows the relationship between pitting corrosion in copper pipes and the presence of carbon films. According to the author,

the carbon films act as efficient cathodes and the remaining surface as an anode, which favors the formation of pits [20]. Some authors point out that localized corrosion in copper pipes is mainly due to the decomposition of the lubricant used in drawing the pipes. Gentil mentions that the lubricant residues remain in the pipe and the lubricant decomposes during annealing to form carbon [9]. More recently, Iysaki's study showed that under the current chemical conditions of water treatment, only the copper pipe with a residual carbon content of $6.1 mg/dm^2$ showed a significant increase in corrosion potential after two weeks and pitting corrosion occurred [21].

2.2.3.3 Soldering flux

In some studies, the presence of soldering flux has been associated with pitting corrosion in copper pipes. According to the literature, the flux used in copper may contain elements with chloride (Cl^-), such as ammonium chloride (NH_4Cl), zinc chloride ($ZnCl_2$), tin chloride ($SnCl_2$) or hydrochloric acid (HCl). The presence of these elements enhances the occurrence of pitting if the flux is introduced into the pipes in excess. Pits tend to occur preferentially along narrow regions that are parallel to the longitudinal axes of pipes and fittings [22, 23].

2.2.3.4 pH

Several authors mention the importance of pH in pitting corrosion of copper. Generally, copper uniform corrosion is associated to low pH and high alkalinity in contrast to copper pitting corrosion is favored in waters with high pH. According to Harold, pitting corrosion is more likely to occur in water with high pH, namely pH 7-9.5 [14, 30].

2.2.3.5 Chloride

Duthtil states that chloride is one of the main causes of pitting corrosion in copper, chloride ion has a very aggressive corrosive effect due to its small ionic radius, which allows greater diffusion between the monolayers formed on the metal surface [27]. In the case of copper, values found in the literature related to the environment are between 0-20 ppm [24].

2.2.3.6 Chlorine

According to the study elaborated by Emily Sarver and Marc Edwards and based on electrochemical data, authors conclude that pits initiated more rapidly with increased levels of free chlorine. The authors concluded that even moderate levels of chlorine, about 0.4 mg/L caused severe pitting on copper pipes [26].

2.2.3.7 Sulfate

Sulfate is considered to be one of the most aggressive anionic species that could lead to copper pitting. According to Farooq the values of sulfate to initiate pitting round 17 ppm [8].

2.2.3.8 Microbial activity

In addition, recent publications in the literature have addressed pitting corrosion in copper caused by microbial activity. Burleigh and his collaborators provided further evidence of the role of microbes in copper pitting corrosion using SEM/EDS. Scanning electron microscopy revealed long tubular structures resembling *actinobacteria* inside copper pits illustrated by figure 2.7. The authors suggest that these bacteria may be involved in acid production that contributes to pit growth [28].

The importance of bacteria in the pitting corrosion process is largely due to the biological and biochemical action and of one particular group: sulfite-reducing bacteria. In this type of attack, sulfides are formed by the action of anaerobic sulfate-reducing bacteria on naturally occurring sulfates during periods of stagnation. In the presence of sulfide ions, copper(II) sulfide (CuS) forms on the metal surface instead of copper oxide II (CuO) and pitting occurs as the sulfides act cathodically on the base of the metal [30].
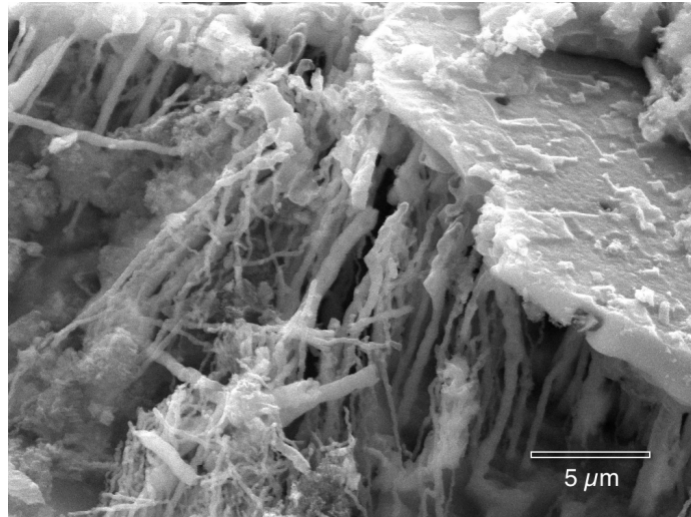
FIGURE 2.7: Microbial filaments inside a copper corrosion pit. Adapted from [28].

2.2.3.9 Water flow

The copper corrosion rate is related to the formation of copper oxide because copper corrosion products form a barrier to the diffusion of cupric ions and oxygen. If the velocity of water flow is higher, the protective layer can detach via erosion. This exacerbates the extent of corrosion occurring at local points exposed to great turbulence. The electrochemical imbalance can also be increased by differential flow as a result of transport near the surface of the pipe that is exposed to more turbulence. The section of the surface with the higher flow is exposed to corrosion reactants than the rest of the pipe as shown illustrated by figure 2.8 [29].
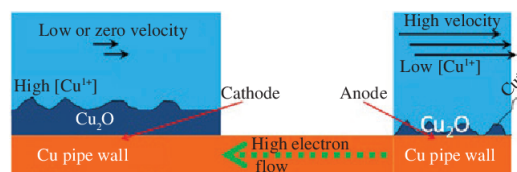
FIGURE 2.8: Schematic of concentration cell pitting corrosion for anodically limited reaction. Adapted from [29].

As mentioned before, the area exposed to high flow will become anodic, and in other situations, the portion will become cathodic. According to Roy, the water chemistry can accelerate pipe failures due to differential flow influenced by the type and durability of oxides that forms on the copper pipes surfaces at the cathode and anode. Water velocity under turbulent flow rate conditions in the section has a significant effect on the protective

layer of copper oxides present on the inner surface of copper pipes as shown by figure 2.9. Variation of copper oxide layer specifications of smoothness, adhesion and stability has effects on copper corrosion resistance in running water environment.

(A)

(B)
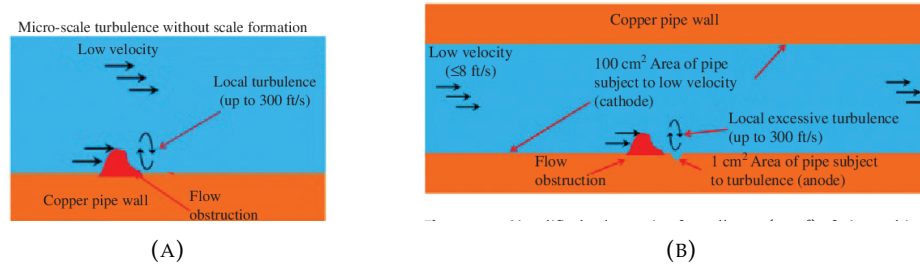
FIGURE 2.9: (A) Schematic of localized high velocity and turbulence, which may form downstream from an obstruction. (B) Simplified schematic of a small area ($1cm^2$) of pipe subject to turbulence and a large area ($100cm^2$) of pipe subject to low velocity. Adapted from [29].

2.3   Eletrochemical Methods to study Pitting Corrosion

The literature points different electrochemical methods to study pitting corrosion, namely: Potencyodinamic Polarization, Electrochemical Impedance Spectroscopy and Electrochemical Noise [19, 31, 32]. A brief explanation of the Open Circuit Potential (was carried out prior to Potentiodynamic Polarization), Potentiodynamic Polarization and Electrochemical Impedance Spectroscopy technique will be addressed since it was used in the experimental work.

2.3.1   Open Circuit Potential

Open Circuit Potential (OCP) is the simplest test that can be performed on an electrochemical system. This technique allows the measurement of the equilibrium potential of the system (which corresponds to the corrosion potential), whose function is to determine when the material (working electrode) reaches its state of thermodynamic equilibrium with time in a given environment. The change in potential is measured over time and in this way, information is obtained about the corrosion potential and the time it takes for it to stabilize. In many applications, there is interest in monitoring the value of the corrosion potential over time, and it is convenient to make a continuous record of the potential variation. This procedure is recommended, especially in the early stages of the experiment.

2.3.2   Potenciodynamic Polarization

Potentiodynamic polarization is a polarization technique in which the potential of an electrode changes at a certain rate and "forces" an electric current pass through an electrolyte. This method provides very useful information about the corrosion mechanisms like corrosion susceptibility of materials in certain environments [9].

The functional dependence between current density and potential is called a polarization curve. A polarization curve can be determined by two different methods: the potentiodynamic method and the galvodynamic method. In the case of the potentiodynamic method, i = f (E) and in the case of the galvanodynamic method, E = f (i), where i is the current through the electrolyte and E is the potential difference between the working electrode and reference electrode.

To obtain a potentiodynamic polarization curve, a potentiostat is required (more detailed information regarding the operation of the electronic circuit of the potentiostat can be found in Appendix A). A potentiostat is an electronic instrument that controls the voltage between a working electrode (WE) and a reference electrode (RE). The potentiostat implements this control by injecting current through a counter electrode (CE). The device controls the current between the working electrode (WE) and the counter electrode (CE) to maintain the potential difference between the working electrode (ET) and the reference electrode (ER) as shown in figure 2.10.
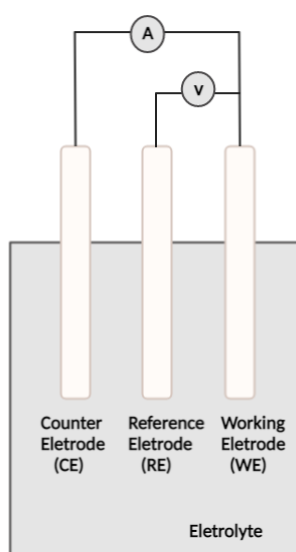
FIGURE 2.10: Schematic of three eletrode setup.

The working electrode (WE) is the electrode where the potential is measured with the respect to the reference electrode (RE). In corrosion testing, the working electrode (WE) is a sample corresponding to corroding metal and the reference electrode should have a constant electrochemical potential as long as no current flows through it. The counter electrode (CE) is a conductor that completes the cell circuit. The electrodes are immersed in an electrolyte (typically an electrically conductive solution).

In order to understand in more detail the electrochemical phenomena associated with corrosion is represented a polarization curve. Polarization curves were traditionally plotted as E vs. current density (i), or alternatively logi. In other words, i was taken as the independent variable. The corrosion potential (E_{corr}), the pitting potential (E_{pit}) and the repassivation potential (E_{rp}) can be obtained from the polarization curve, as illustrated by

figure 2.11. The pitting resistance can be compared and predicted based on the magnitude of the values and the relative position of the pitting potential compared to the corrosion potential. If the value of the pitting potential is positive compared to the corrosion potential, the pitting resistance of the material is high [33].
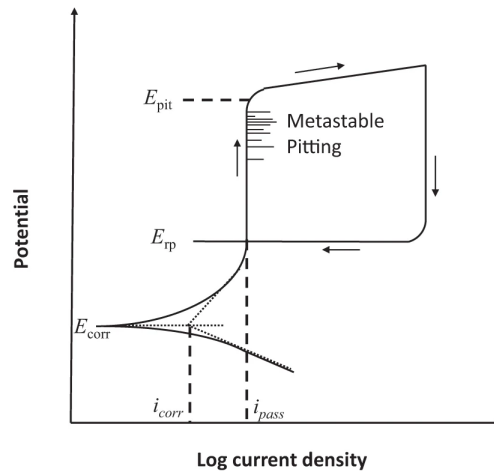
FIGURE 2.11: Illustration of a polarization curve. Adapted from [33].

The pitting potential can be determined by the intersection of the tangent to the curve before the abrupt increase in current density with the tangent to the curve after this change. This determination of the pitting potential becomes simple when the polarization curve exhibits a significant change in direction. In some cases, the change in current density values is less pronounced, making it difficult to use this technique to determine the pitting potential.

2.3.3   Eletrochemical Impedance Spetroscopy

Electrochemical impedance spectroscopy (EIS) is an electrochemical technique that has been used to study the corrosion behaviour, passivation and coatings for different materials [34]. The ultimate purpose of the EIS is to obtain information about the protective properties of the coating/passive film, such as the presence of defects, interface reactivity, adhesion or water barrier properties. The knowledge of these parameters, therefore, is very useful in the prediction of the behaviour of the film formed, providing a detailed view of the electrical characteristics of the electrode/electrolyte solution interface. This technique consists in applying an AC potential of a small excitation signal and measuring the electric current as illustrated by figure 2.12.
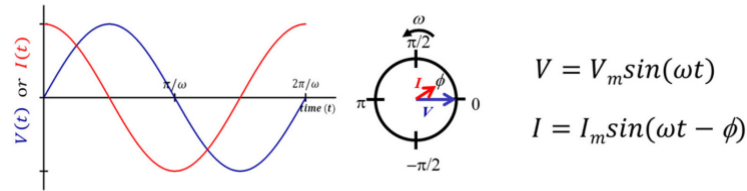
FIGURE 2.12:   The illustration and equation about the relationship between the voltage and current when applying an AC potential with the angular frequency ω. Adapted from [34].

The excitation signal is expressed in equation 2.3 as a function of time, where V_t is the potential in instant t, V_0 is the potential of the signal and w is the angular frequency ($\omega = 2\pi$f) of the applied potential. The applied potential has the same value of the equilibrium potential of the system corresponding to Open circuit Potential (OCP). The response of the system is a sinusoidal current shift phase I_t in instant t with a phase ϕ as expressed by equation 2.4.

$$V_t = V_0 sin(\omega t) \tag{2.3}$$

$$I_t = I_0 sin(\omega t - \phi) \tag{2.4}$$

An expression analogous to Ohm's law allows to calculate the complex impedance of the system as the ratio of input V_t and output measured current I_t :

$$Z = \frac{V_t}{I_t} = \frac{V_0 sin(\omega t)}{I_0 sin(\omega t - \phi)} \tag{2.5}$$

If we plot the applied sinusoidal voltage signal on the x-axis of a graph and the sinusoidal response signal I_t on the y-axis, an oval figure known as a "Lissajous figure". Through the relationship of Euler is known that:

$$e^{j\phi} = cos(\phi) + jsin(\phi) \tag{2.6}$$

$$V_t = V_0 e^{j\omega t} \tag{2.7}$$

$$I_t = I_0 e^{(j\omega t - \phi)} \tag{2.8}$$

$$Z = Z_0 cos(\phi) + jZ_0 sin(\phi) \tag{2.9}$$

The EIS graphical representation can be typically represented in two ways: Nyquist diagrams and Bode diagrams. The Nyquist diagram can be plotted, where typically the imaginary component of Z is represented on the y-axis and the real component of Z on the x-axis as shown in equation 2.9. The Bode Diagram can be represented in polar coordinates Z (y-axis) and phase angle (y-axis) as a function of frequency $\omega = 2\pi f$ (x-axis), this diagram allows detecting subtle variations in the system. The Bode plot has great advantages for observing phase margins in which the system becomes unstable (intense phase or magnitude changes) [34].

The best way to understand the results of EIS is through the analysis of equivalent electric circuits, given that an electrochemical system can be modeled using passive elements like resistances, capacitors and inductors [35]. The equivalent element, symbol, impedance and physical process of an equivalent circuit that avoid to describe the behaviour of kinetic of electrochemical reactions are described in table 2.2.

TABLE 2.2: Circuit elements used in the equivalent circuit. Adapted from [34, 35].

Equivalent Element	Symbol	Impedance	Physical Process
Resistance	R	$Z = R$	Load transfer
Capacitance	C	$Z = \frac{1}{j}\omega C$	Double electrical layer
Inductance	L	$Z = j\omega L$	Charge adsorption
Warburg Impedance	W	$Z = \frac{\sigma_i}{\sqrt{w}}(1-j)tanh\sqrt{\frac{jw}{D_i}}$	Diffusive mass transport
Constant Phase Element (CPE)	Q	$Z = \frac{1}{C(jw)^n}$	Models the behaviour of a double layer

σ_i is coefficient of Warburg.

Using as examples R, L and C for simple electric circuits. The first equivalent element represented in table 2.2 is a resistor and impedance is a result of no phase shift ($\phi = 0$) corresponding to R. There is visible in the Bode plot a constant parallel to abscissa as represented by figure 2.13 for resistances with R = 100 Ω, 500 Ω and 1000 Ω.
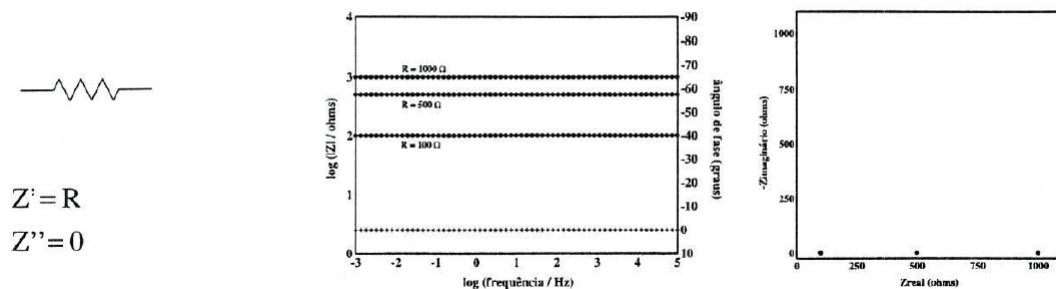
FIGURE 2.13: Bode and Nyquist Diagram for resistances R = 100 Ω, 500 Ω and 1000 Ω. Adapted from [36].

The second equivalent circuit represented in the table above is capacitance and is related to the double electric layer. Capacitance has the capacity to store charge. It is visible in the Bode plot represented by figure 2.14 capacitances with capacities of C = 1 pF, 1nF and 1 μF.
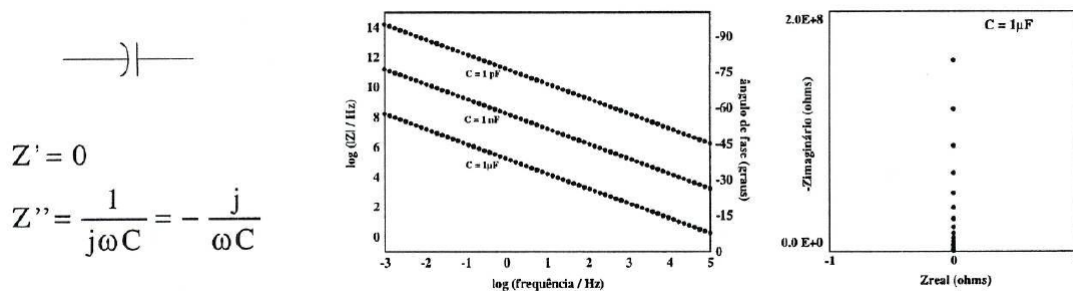
FIGURE 2.14: Bode for capacities C = 100 pF, 1nF and 1 μF (left) and Nyquist Diagram with C = 1 μF (right). Adapted from [36].

The third equivalent circuit represented in the table is inductance. Inductance has only an imaginary component and impedance is a result of phase shift ($\phi = 90°$) with respect to the voltage corresponding to jωL and is related to charge absorption. Figures 2.15 show different inductances for L = 1000 H, 1 H and 0.01 H (left).

$$Z' = 0$$
$$Z'' = j\omega L$$
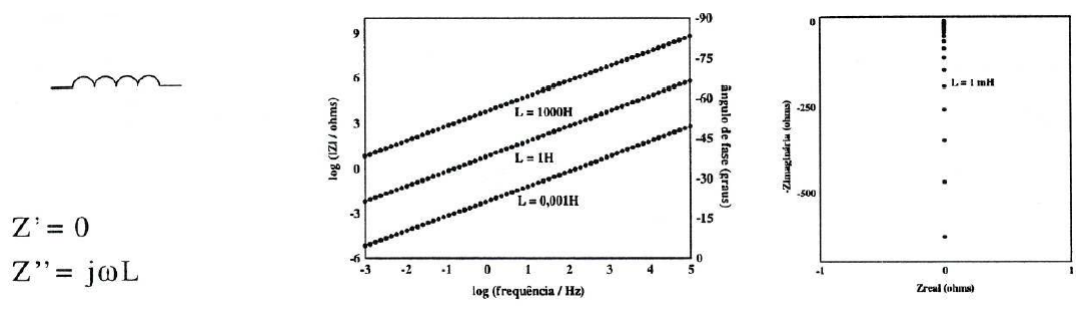
FIGURE 2.15: Bode for inductances L= 1000 H, 1 H and 0.01 H (left) and Nyquist Diagram with L = 1 mH (right). Adapted from [36].

It is important to point out that the same equivalent electric circuit model can fit experimental data from different systems. Therefore, it is essential to have prior knowledge of the physical phenomena involved in the system under study, in order to perform a correct adjustment of experimental data obtained by the EIS technique and the equivalent electric circuits model selected [37].

Chapter 3

Manufacturing Process Overview

This chapter focuses on the analysis and description of the manufacturing process of the heat exchangers used in gas water heaters. The monitoring of the manufacturing process was divided into seven phases: skirt manufacturing, coils manufacturing, elbows and U-pipes manufacturing, assembly of components, furnace brazing and functional test.

3.1 Analysis of the manufacturing process of heat exchangers

This phase of the work was carried out in the production section of Bosch Thermotechnology, S.A - Aveiro, with the main purpose of monitoring the manufacturing process of the heat exchangers. The analysis of the manufacturing process was carried out through the acquisition of three types of data: observations, interviews and analysis of documentation. Initially, observations were carried out that made it possible to understand in real context the respective phases of the manufacturing process of the heat exchangers. Interviews were also carried out with members of production, quality and engineering. Bosch standards, European standards and documentation provided by suppliers were analysed.

Structurally, a heat exchanger is made up of seven important components: skirt, cold water coil, hot water coil, fins, U-pipes, turbulator and elbows as illustrated by figure 3.1. The raw material of choice for heat exchanger manufacturing is copper, given its high thermal conductivity and high plastic conformability.
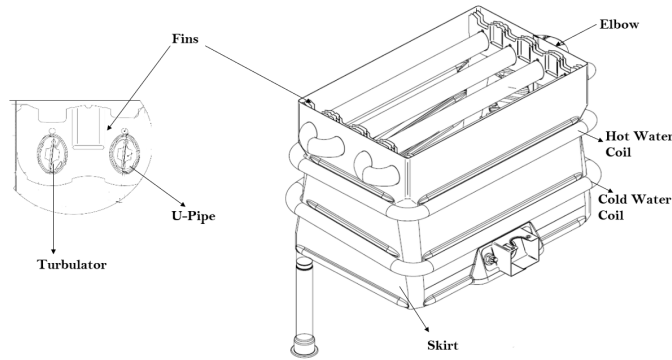
FIGURE 3.1: Structural composition of a heat exchanger used in gas water heaters.

The skirt is the component that gives shape and strength to the heat exchanger and functions as a casing, in which combustion takes place inside. The skirt has a rectangular geometry and is helically wrapped by a cold water coil and a hot water coil. The helical shape of the coils aims to cool the walls of the heat exchanger, preventing phenomena such as thermal fatigue.

The skirt is surrounded by coils. The coil that carries the water to the U-pipe is called a cold water coil since the water that circulates in it is at a relatively low temperature (around 10-25°). On the other hand, the coil that carries the water from the U-pipe for the plumbing network is called a hot water coil, as it transports hot water (around 35-50°).

The upper region of the heat exchanger is composed of four pipes, fins arranged in parallel and a turbulator. The function of the turbulator, as the name implies, is to create turbulence, increasing the molecular agitation of the water inside the pipe.

3.1.1   Skirt manufacturing

Firstly, the manufacturing process of the component that gives strength to the heat exchanger will be described: the skirt. The Bosch N28 standard - Material order and specifications were carefully analysed, in order to understand the chemical composition, material conditions and mechanical properties. Regarding the chemical composition of the copper used to manufacture the skirt, it has a percentage of 99.90 % of copper (Cu) and 0.015-0.040% of phosphorus (P). Mechanical properties described in the standard were analysed, namely: tensile strength, elongation after fracture in % and hardness, the values are described in the table 3.1 [38].

TABLE 3.1:   Mechanical properties of copper used in skirt manufacturing according to the Bosch standard Bosch-NormContent.

Parameter	Value	Unit
Tensile strength	220 to 260	MPa
Elongation after fracture in %	min.(33)	-
Hardness	55	HB

Copper, as shown in figure 3.2, is produced in a roller, which is formed and cut in a press, creating a "patina"(name assigned in the production section). The sheet is then folded and then opened to give the apron the desired shape. The joining of the sheet is done by a process called "stitching". In this process, the ends of the sheets are bent to intertwine them together.

FIGURE 3.2:   Raw material used for skirt manufacturing.

3.1.2 Coils manufacturing

In this subchapter, the manufacturing process of coils will be described (cold and hot water coils), highlighting the material properties. The mechanical properties of the material were analysed, as shown in the table 3.2 [39].

TABLE 3.2: Mechanical properties of copper used in the coils manufacturing according to Bosch standard [39].

Parameter	Value	Unit
Tensile strength	220 to 260	MPa
Elongation after fracture in %	min.(52)	-
Hardness	55	HB

The non-uniformity in the wall of the pipes was analysed, and the corresponding max allowed value is ±0.01 mm. Special emphasis was given to the analysis of the carbon values allowed by the standard. According to the standard the carbon values are also controlled, and the carbon values must be less than 20 mg/dm^2 according to the Bosch internal standard.

The raw material arrives at the production section in coils as shown in figure 3.3. The dimensions of the external diameter and thickness of the coils are 13.00 x 0.60 mm, respectively.

FIGURE 3.3: Raw material used for coils manufacturing.

The coil is introduced by the employee in the corresponding coil production machine to carry out the desired design. The manufacture of hot and cold water coils is carried out in two similar machines, one of the machines designing the cold water coils and the other one for hot water represented in the figure 3.4. The machines mentioned above are based on a Computerized Numerical Control (CNC) that works in three axes: translation in x (the x value gives the value of each of the straight sections of the coil), rotation in y (the y value indicates the value of the angle that each of the straight sections makes with the fixed reference) and rotation in z (the value of z gives the angle that two straight sections give to each other) represented in figure 3.4.

FIGURE 3.4: Machine used for coils manufacturing.

Next, the end of the cold water coil is squashed to allow it to fit into the upper region of the heat exchanger. The oil used for the conformation of the end of the cold water coil is Lubsec (the datasheet of oil is attached in appendix B). The application is made using a spraying system as shown in figure 3.5.

FIGURE 3.5: Cold water coil: flare formation.

3.1.3   U-pipes and elbows manufacturing

U-pipes and elbows are mechanically deformed to obtain the final shape and is used
Polyethylene glycol 400 oil to assist mechanical deformations. After this procedure, these
components are washed in a machine designed for this purpose with Gardoclean ®A55103
cleaner.

3.1.4   Assembly of components

In the assembly cell, the components are assembled. Components are mechanically and
manually coupled in order to ensure that the heat exchanger is in its final shape. Firstly,
the fins block is assembled in the top of the heat exchanger, jointly with the U- pipes and
the turbulator. In the next phase, the cold and hot water coil are mounted on the skirt,
ensuring that they are as tight as possible to the skirt.

3.1.5   Furnace Brazing

In this subchapter is discussed in detail the furnace brazing process, including geome-
try, operation of the oven, temperature profile and welding paste will be presented. This
process guarantees the union between the coils and the skirt of the heat exchanger. Ac-
cording to the American Welding Society (AWS), brazing is defined as a group of joining
processes that produce coalescence of materials by heating them to high temperatures,

usually above 450°C, using a metal of addition that melts at a lower temperature than the base material.

The oven used for furnace brazing at Bosch Thermotechnology is a large oven intended for the production of around 1500 heat exchangers per day. A better understanding of oven geometry can be obtained through the figure 3.7. The equipment has a rectangular shape and has a length of approximately 25m. The oven has a single burner located in the initial part. The oven atmosphere is composed of a mixture of 95% of Nitrogen (N_2) and 5% of Hydrogen (H_2), with an injection rate of the gas mixture of approximately 93 m^3h^{-1}. The permanence time of each heat exchanger inside the oven is approximately 45min.

Commercial nitrogen-based industrial furnace atmospheres are technically acceptable for most metal processes. This element serves as a pure, dry and inert gas, providing a protective atmosphere by preventing oxidation or decarburization of the metallic surface during heat treatment.
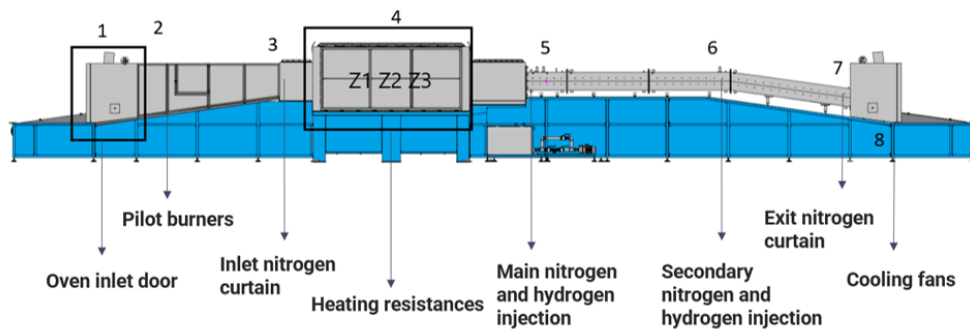
FIGURE 3.6: Schematic representation of oven used in the production section of Bosch Thermotechnology.

Figure 3.7 shows the temperature distribution as function of time and distance of the oven. The different colors present in the temperature profile indicate the positioning of the temperature sensor in the copper heat exchanger. The values of temperature reached by copper passing through the oven in region Z3 are mentioned in table 3.3.

TABLE 3.3: Temperature reached by copper passing through the oven in region Z3.

Point of application	Temperature (°C)
1	824.3
2	820.4
3	828.8
4	798.7
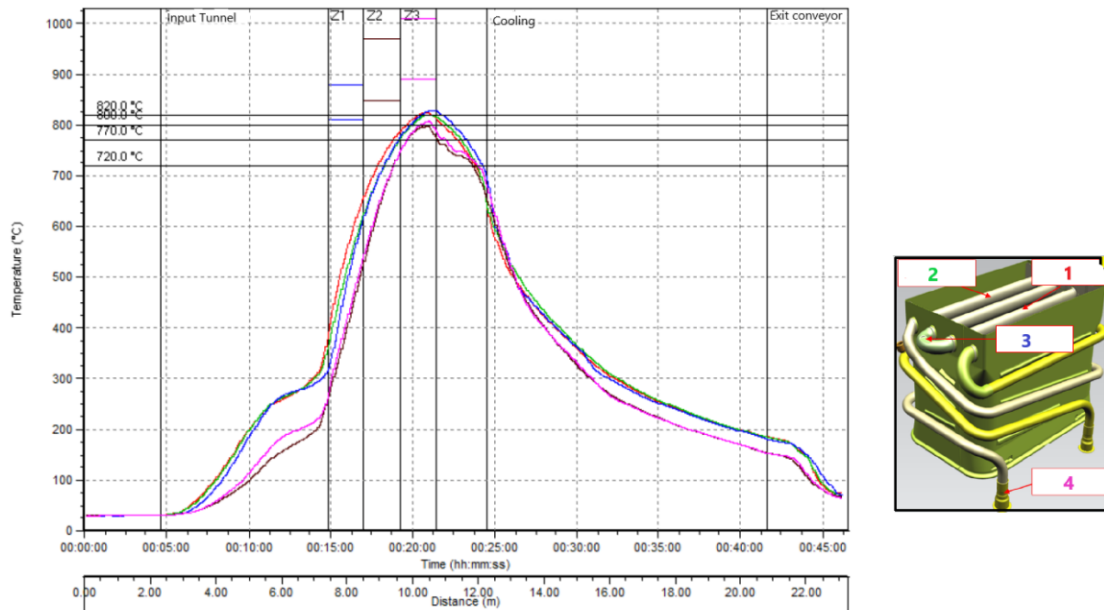
FIGURE 3.7: Schematic representation of temperature profile of oven used in production
section and point of application of temperature sensors in the heat exchanger.

In the temperature profile, there are three distinct regions called Z1, Z2 and Z3, which refer to the oven heating values. The region called Z1 temperature varies between 780°C and 800°C, Z2 varies between 830°C and 860°C and Z3 varies between 910°C and 930°C. Analyzing the maximum temperature values of the heat exchanger it is observed that the maximum temperature reached by copper is 828.8° in the region Z3 of the oven. The maximum oven temperature maximum occurs after 26 min.

The filler materials currently used are solder rods in the straight sections of the heat exchanger and welding paste at several points of the coils. The welding paste consists of copper phosphorous (CuP) alloy and binder. Phosphorus (P) composition varies between 7.5-8.1%, and the melting temperature of the respective solder is about 710 to 770ºC. Currently, the composition of the binder is not known. After the respective application of the rods and solder paste, the chambers are placed on a steel gauge (which supports the heat exchanger) and positioned on the conveyor belt at the oven inlet.

3.1.6 Dry test

After the Furnace Brazing process, all heat exchangers are tested in a Dry test system represented in figure 3.8. This test ensures that heat exchangers don´t have internal leaks. During the test, the test piece is first filled with air to a pre-set pressure. After the filling step, stabilization takes place. Stabilization is one of the most important stages of the entire process, having a direct impact on the quality of the results obtained later on. As a rule, depending on the volume and geometry of the body, this is usually the longest stage of the entire process. Then, at the end of stabilization, the measurement takes place, this step measures during a previously defined time interval the pressure variation inside the heat exchanger $\Delta P / \Delta t$ as shown in the following figure:

(A)

(B)
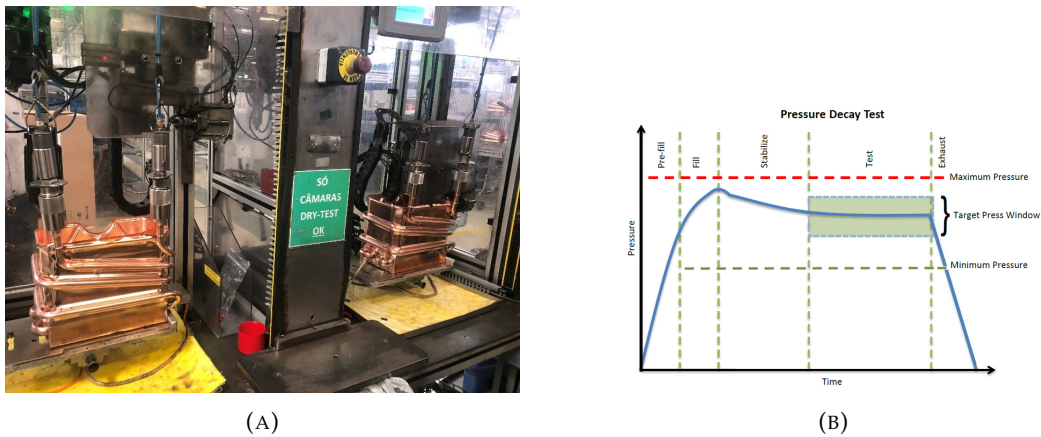
FIGURE 3.8: (A) Dry test system used for leak detection. (B) Pressure Decay Diagram.

Its operating system is relatively simple, compact and user-friendly. The acquisition is relatively cheap and the operating costs are only associated with the consumption of compressed air, which makes the test dry and clean, not damaging or adding additional cleaning costs after a leak test, combined with the fact that there is no need for any judgment on the part of the operator as to the test result, it is only necessary to follow the guidelines of OK, or NOK.

3.1.7   Functional test

In the final line of the manufacturing process of gas water heaters are carried out the final tests, also known as functional tests. During the performance of the functional test, the gas water heater is already fully assembled and is carried out prior to the packaging. During the functional test, initially, a test is carried out on the water circuit, ensuring that there is no type of water leak, followed by the test on the gas circuit. In the third phase, the appliance is tuned, ensuring that its power is similar to the values previously established.

After the respective adjustment, the operation of the safety components of the gas water heater is verified, causing failure situations and analyzing the response of the appliance. In this phase the hot water outlet valve is closed and the water heater is checked. Then the hot water outlet valve is opened again, verifying that the water heater is turned on again, starting the burning through the pilot burner, which will then ignite the remaining burner. With the water heater in operation again, the thermostat heats up, which detects the return of combustion gases and the water heater switches off.

If the gas water heater passes all tests, it moves to the next station where it is packed and ready for shipment to the final customer. However, when the appliance does not pass the final test, it is reworked, trying to repair the problem detected.

The total duration of the leak test is approximately 2 min. During the tests, the limits are previously established for the passing criterion: the nominal water pressure varies between 2.3 and 2.7 bar and maximum water flow between 12.0 and 16.0 l/min. At the end of the test, is performed a purge with a duration of 5-10s.

Considering the test is performed with recirculated water and the purge time is quite short, the chemical parameters of the water used in the functional tests will be investigated. A Tree Diagram represented in figure 3.9 was used in a top-down way, to detail pitting corrosion failure in successive levels considering possible causes for pitting corrosion in copper heat exchangers.
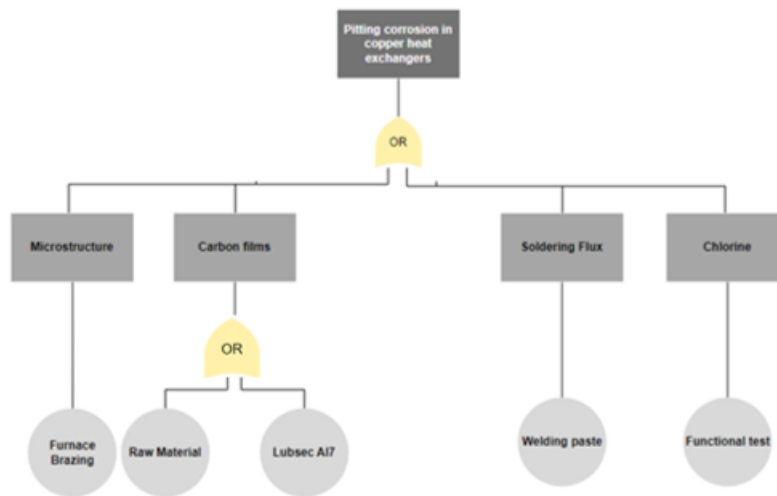
FIGURE 3.9: Fault tree analysis of manufacturing process: possible causes for pitting corrosion in copper heat exchangers.

At the top of the fault tree analysis, we have the fault that is pitting corrosion in copper heat exchangers. In the second branch we have some of the causes found in the literature previously mentioned in the state of the art, namely: microstructure, carbon films, soldering flux and chorine. In the third branch we have the possible sources taking into account the manufacturing process of heat exchangers from Bosch Thermotechnology previously described.

In the figure 3.9 we have as a first possible cause for pitting corrosion in copper heat exchangers the microstructure, due to the fact that in the manufacturing process of heat exchangers possibly there are microstructural changes during the process of furnace brazing. The second possible cause are carbon films, which are subdivided into two branches: the raw material and the Lubsec. The raw material naturally contains carbon from the copper extrusion process and the oil Lubsec contains hydrocarbons in its chemical composition.

The third possible cause is the soldering flux, given that the welding paste is applied directly in copper coils of the heat exchanger. The fourth cause mentioned is chlorine, since during the functional tests is used recirculated water, so it could be a source of chlorine contamination.

Chapter 4

Materials and Methods

This chapter exposes the materials used, as well as the methods used in the experimental work. In order to achieve the proposed goals, the experimental work was carried out in three distinct phases as can be verified by the figure 4.1. The first phase consisted in the preparation of samples for analysis of pits present in the external and internal section of a heat exchanger that was in operation. The second phase consisted in mettalographic preparation of different copper samples taken from the coils of several heat exchangers in order to characterize from a microstructural point of view different copper samples that will be studied later. In a third phase, electrochemical experiments were carried out using samples with different provenances, using potentiodynamic polarization, electrochemical impedance spectroscopy and SEM/EDS, in order to study the root causes related to the Manufacturing Process.
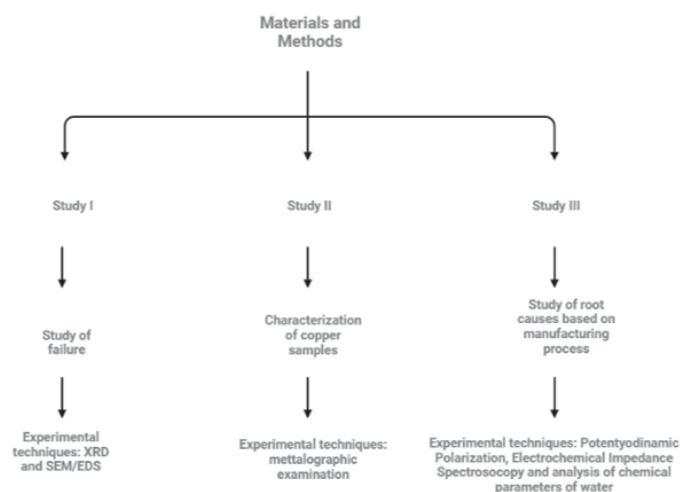
FIGURE 4.1: Diagram corresponding to the three distinct phases of the experimental execution.

4.1 Preparation of samples for analysis of pits

The first experimental point covers the characterization of pits present in the external and internal surfaces of a heat exchanger that exhibited pitting corrosion in coils. The heat exchanger under study has a capacity of 14L and has been in operation during 15 months in Germany, in the city of Kohn. Firstly, the different sections of the coils of the heat exchanger were identified and recorded, taking into account the different views of the heat exchanger as represented in figure 4.2. In table 4.1 is presented the designation assigned to each section, as well as the corresponding coil.

(A)

(B)

(C)

(D)
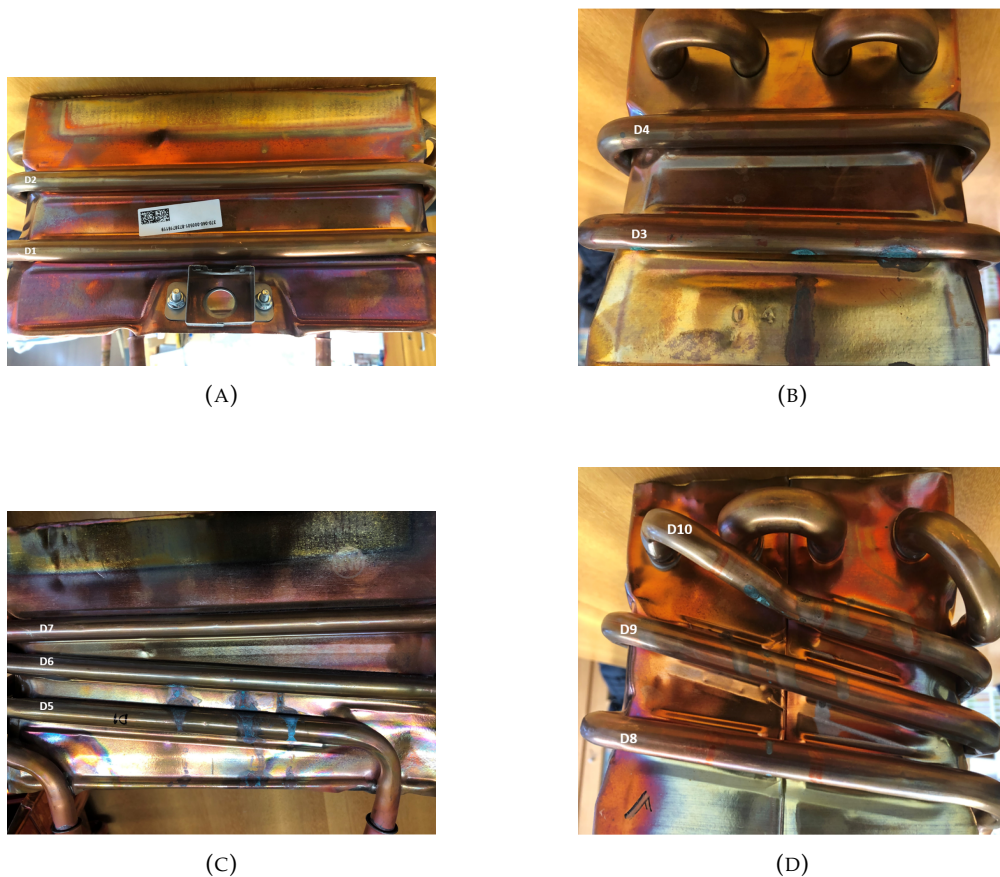
FIGURE 4.2: Different view of heat exchanger (A) Front view: sections identified as D1 and D2. (B) Lateral view: sections identified as D3 and D4. (C) Back view: sections identified as D5, D6 and D7. (D) Lateral view: sections identified as D8,D9 and D10.

TABLE 4.1: Designation assigned to each coil of the heat exchanger with pitting corrosion.

Designation	Corresponding coil
Section D1	cold water coil
Section D2	hot water coil
Section D3	cold water coil
Section D4	hot water coil
Section D5	hot water coil
Section D6	cold water coil
Section D7	hot water coil
Section D8	cold water coil
Section D9	hot water coil
Section D10	cold water coil

4.1.1 Analysis of external surface

After the different sections of the heat exchanger were properly identified and sectioned, the observations were made in stereomicroscopy using a binocular magnifying glass with an automatic exposure system and digital image acquisition of model ZEISS STEMI 200C illustrated by the figure 4.3. Stereomicroscopic photographs were recorded in the case where the appearance of corrosion products was clearly evident on the external surface of the heat exchanger. Observations and acquisition were carried out at the Department of Metallurgical and Materials Engineering of the University of Porto.
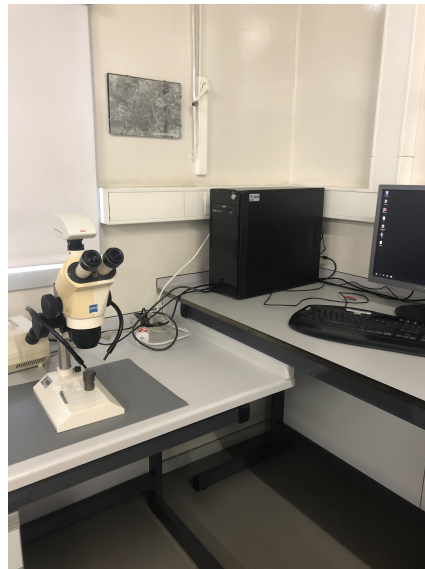
FIGURE 4.3: Stereoscopic microscope with automatic exposure system and digital image acquisition model ZEISS STEMI 200C used for recording corrosion products.

After the acquisition and recording of the stereomicroscopic photographs of the external surface of the heat exchanger, the XRD analysis of the external corrosion products present in the surface was performed using the Rigaku SmartLab diffractometer, located in the Department of Physics of the University of Porto. In the sample preparation, the corrosion products were collected from the heat exchanger and milled until the crystallites were as small as possible. The sample was inserted in the sample holder and using the glass slide the surface was grinding until it was as thin as possible. The crystal structures analysis was carried out by X-ray diffraction at room temperature using Cu-Kα radiation (λ = 1.540593 Å) powered at 45 kV and 200 mA and the Bragg–Brentano θ -2θ geometry in the 2θ range 10°-90º, with a step of 0.01° and scan rate of 12° min^{-1}. The software used to analyse the experimental results was X'Pert HighScore Plus.

4.1.2   Analysis of internal surface

In order to study the morphology of the copper pits present in the internal surface of copper coils of a heat exchanger that was in operation SEM/EDS analysis was performed to observe the pits. The SEM is an equipment that uses highly energized electrons to scan the surface of the sample under study. Due to the interaction between the electrons and the sample, a variety of signals are generated, revealing the external morphology, chemical composition, crystal structure and orientation of the materials constituting the sample. Analysis of pits were carried out using SEM/EDS at Materials Centre of University of Porto (CEMUP), at the Imaging, Microstructure and Microanalysis Unit Laboratory (IMICROS). SEM/EDS analysis was performed on a high-resolution scanning electron microscope (Schottky) with X-ray microanalysis and backscattered electron analysis, using the FEI Quanta 400 FEG represented in figure 4.4.

FIGURE 4.4: CEMUP/IMICROS Scanning electron microscope. Adapted from [40].

The characterized samples were coated with Au/Pd (Gold/Palladium) thin film, in order to guarantee that samples had good electrical conductivity. The sample preparation technique used was sputtering, using the SPI Module Sputter Coater equipment. SEM micrographs were taken with different magnifications, namely: 500x, 1000x and 2000x magnifications. The energy of the electron beam was 15 keV. The surface morphology of the samples was evaluated with the secondary electron detector (SE) and backscattered electrons (BSE). SEM images were also obtained with the backscattered electron detector (BSE) for showing better contrast between materials with significant differences in atomic weights and EDS analysis was used to identify elements.

4.2   Metallographic preparation

The first point of the experimental work concerns the metallographic preparation, with the goal of characterising from a microstructural point of view different copper samples from different provenances, which will be studied throughout this work. The characterized samples were taken from different heat exchangers provided by Bosch Thermotechnology. The table 4.2 shows the designation assigned to each of the samples, as well as their respective provenance.

TABLE 4.2:   Sample designation and provenance of the analysed samples in metallographic preparation.

Sample Designation	Provenance
Cu_Raw Material	Heat exchanger before oven inlet
Cu_Furnace Brazing	Heat exchanger after oven outlet
Cu_Operation_pit1	Heat exchanger that was in operation: region 1 with pit
Cu_Operation_pit2	Heat exchanger that was in operation: region 2 with pit
Cu_Operation _without pit1	Heat exchanger that was in operation: region 1 without pit
Cu_Operation _without pit2	Heat exchanger that was in operation: region 2 without pit

Samples with the designation "Operation" come from a heat exchanger that was in operation in Germany during 12 months. After the heat exchangers were received, the site was chosen for microstructural characterization, taking care to choose the same section of heat exchanger so that the comparative analysis can be judicious.

The coils of the heat exchangers previously selected for microstructure characterization were initially cut into several sections. After the sections were properly sectioned, the areas of interest were duly cut in cross-section with an aluminum oxide disc of Strues with a diameter of 200 mm and a thickness of 0.8 mm. Cutting was performed using a speed of 3000 rotations/min.

After cutting cold assembly was carried out. The cold assembly makes easier to handle the samples and avoid damaging the sandpaper or polishing cloth. The samples were placed in the molds and filled with fast-polymerization synthetic resin, using 100 ml of resin and 10 ml of hardener and were mixed for assembly. The hardening time was about 12 hours. The samples were duly identified in the area behind the samples in order to avoid inconveniences during the metallographic characterization process and properly stored in the desiccator. The prepared samples are represented in figure 4.5.

After assembling the samples, the sandpaper phase followed, whose main goal is to eliminate risks and deeper damages on the surface of the material. Due to the degree of
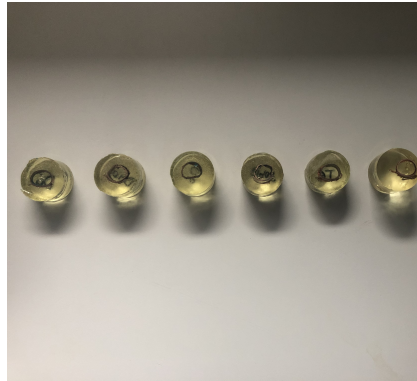
FIGURE 4.5: Metallographic preparation of copper samples for metallographic characterization.

perfection required in the metallographic preparation, the polishing step was carefully prepared. For the polishing, the sequence of silicon carbide (SiC) sandpaper granulometries were: 180, 320, 600, 1000 and 4000 mesh. For each sandpaper subsequent to the first, the sample was rotated 90º, in order to eliminate the scratches left by the previous sandpaper. This step was carried out manually with the Struers polisher at a speed of 300 rotations/min, using water as a lubricant.

After the sanding phase and prior to polishing, the surface of the samples was cleaned in order to remove the impurities present on the surface. The samples were placed in a beaker with ethanol (C_2H_6O) and sonicated for 3 min. After the samples were properly cleaned, polishing was carried out, this phase aims to ensure the surface finish is free from scratches. Diamond suspension with a dimension of 1 μm was used with the polisher at a rotation of 150 rotations/min. Typically for mechanical polishing, diamond is used, taking into account its characteristics of grain size, hardness, grain shapes and grinding. After finishing the polishing step, ensuring that there are no visible risks through observation under an optical microscope, the samples were cleaned with ethanol (C_2H_6O).

Finally, the samples were subjected to chemical attack. The chemical attack was selected taking into account the goal: exhibit the grain boundaries. The chemical attack was carried out in the fume hood, so that it could be carried in a safe way. The following etching was used to reveal the grain boundaries: 25 ml of distilled water, 25 ml of ammonia (NH_3) (25%) and 5 ml of hydrogen peroxide (H_2O_2) (3%), based on [41]. The attack method was by immersion, where the sample was submerged 10s-15s to reveal grain boundaries. After the etching, the sample was rigorously cleaned with distilled water and dried with compressed air.

After chemical etching copper samples were observed by optical microscopy using optical microscope ZEISS Axiotech illustrated in figure 4.6. Photomicrographs of the samples were obtained with an image acquisition program Leica Application Suite (LAS) using CCD camera system coupled to the microscope. Observations and acquisition were carried out at the Department of Metallurgical and Materials Engineering of the University of Porto. Due to the impossibility of using the grain expert tool, which allows automatic identification of the grains, was used a manual image processing program, namely Image J.

FIGURE 4.6: Optical Microscope ZEISS Axiotech used to record different microstructures of copper samples.

4.3   Eletrochemical experiments and characterization of samples

4.3.1   Potentiodynamic Polarization

The second point of the experimental work concerns the potentiodynamic polarization experiments. The main focus was studying copper samples (Cu-DHP) in different conditions and environments in order to evaluate pitting resistance. In order to simulate different environments with high chloride and sulfate concentration 2 test solutions were used: test solution with 0.6 M of sodium chloride (NaCl) as described by the standard ASTM G61-86 [42] and test solution of 0.1 M of sodium sulfate (Na_2SO_4).

In order to reproduce experimentally the different transformations that copper coils undergo during the manufacturing process of the heat exchangers, a procedure was developed for sample preparation. Three different types of samples were prepared, with particular attention to the application of Lubsec oil and the furnace brazing process. Figure 4.7 illustrates the preparation of the different copper samples in order to reproduce real conditions in an industrial context.
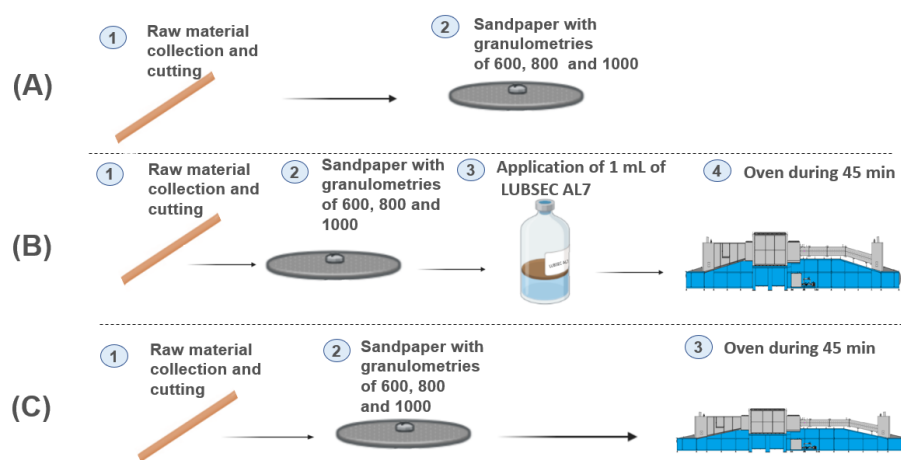
FIGURE 4.7: Schematic representation of procedure for preparation of different copper samples. (A) Copper (Cu - DHP) corresponding to raw material. (B) Copper (Cu-DHP) with an application of 1mL of Lubsec using volumetric pipetting and passing through the oven during 45 min. (C) Copper (Cu-DHP) passing through the oven during 45 min.

The copper samples (Cu-DHP) used as a working electrode during the potentiodynamic polarization experiments were collected in the production section in the form of pipes as shown in figure 4.8. After collection, the pipes were sectioned into approximately equal portions: 6 cm and cut in half. The samples were polished with silicon carbide (SiC) sandpaper with granulometries of 600, 800 and 1000 mesh to remove any imperfections present in the samples.

In the case where it was intended to study the influence of the use of Lubsec oil (Figure 4.7 B)), 1 mL of the oil was measured using a volumetric pipette and applied in the internal section of the pipe. After the application of the oil, it was waited 1 hour before putting the samples in the oven.

Next, the copper samples were drilled and tin-welded to make electrical contact. Samples were coated with epoxy resin ensuring that the area exposed to the electrolyte was constant (1 cm^2), as shown in the figure 4.8 B). The use of epoxy resin had as main goal to expose only the area under study so that it is constant, and electrically isolates the remainder of the sample. For this purpose, was used commercial epoxy resin "araldite", applying the proportion 1:1, respecting 1 of resin for 1 of hardener to ensure proper hardening.

(A)
(B)
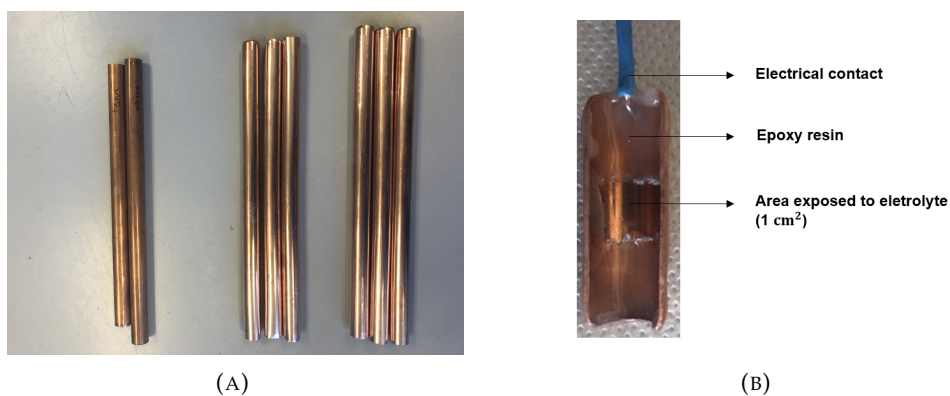
FIGURE 4.8: Preparation of samples for polarization tests. (A) Copper pipes used for sample preparation. (B) Example of sample preparation for potentiodynamic polarization experiments making an electrical contact tinned welded and coating with epoxy resin.

To carry out the electrochemical experiments, it was necessary to size the electrochemical cell and the sample holder represented in figure 4.9, given the morphology of the copper samples. The electrochemical cell was drawn ensuring that the distance between the electrodes is constant and that are relatively close together, the dimensions are in Appendix D.

FIGURE 4.9: Electrochemical cell and sample holder drawn for electrochemical experiments using as print material ABS P340.

The equipment used during the electrochemical experiments included a Gamry potentiostat of model Interface 1000 illustrated in figure 4.10 A). The experiments were controlled and the results were recorded using the Gamry Framework software in a computer connected to the potentiostat. A conventional three electrode electrochemical cell was used: working electrode (WE), reference electrode (RE) and counter electrode (CE). The working electrode was prepared from copper pipes as described previously. The reference electrode used was the most widely used in laboratory experiments and was made up of Silver/Silver chloride (Ag/AgCl), immersed in an electrolyte saturated with 3 M of Potassium Chloride (KCl). The counter electrode used was a platinum (Pt) wire.

(A)   (B)
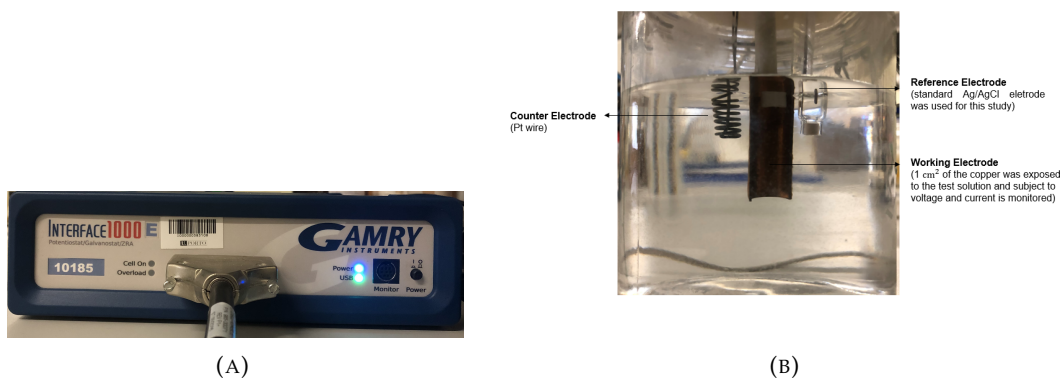
FIGURE 4.10: (A) Potentiostat Gamry Interface 1000. (B) The electrochemical cell which can be attached to either system.

The established parameters, listed below, were based in the literature. The open circuit potential was recorded for a time of 3000s to achieve equilibrium between the sample and the environment. The potential range studied is between the values - 0.5 and 1.2 V in relation to the open circuit and the sweep speed used was 0.167 mV/s, based on [42]. After each experiment, the samples were observed under an optical microscope to identify the region of pit formation. Prior to testing, a cathodic potential was applied to the working electrode for 2 min to remove any trace of air-formed oxide on the metal surface).

4.3.2 Eletrochemical Impedance Spectroscopy

During the experiments of electrochemical impedance spectroscopy were used samples with different provenances and two test solutions. Samples were the following: copper (Cu - DHP) corresponding to raw material, copper (Cu-DHP) with application of 1mL of Lubsec AL7 and passing through the oven during 45 min and Copper (Cu-DHP) passing through the oven during 45 min. The procedure for samples preparation was the same as those used in the potentiodynamic polarization and were used two different test solutions namely 0.6 M of sodium chloride (NaCl) and 0.1 M of sodium sulfate (Na_2SO_4).

The open circuit potential was recorded for 3000s. A 10 mV rms sine perturbation was applied in turn of the OCP in the frequency range of 10^5 to 10^{-3} Hz with 7 points per decade with logarithmic distribution. The EIS tests were performed with a potentiostat Autolab PGSTAT302N with the aid of the software Nova software. The electrochemical experiments were performed at the Department of Materials of the University of Aveiro. The setup used is represented in the figure 4.11.
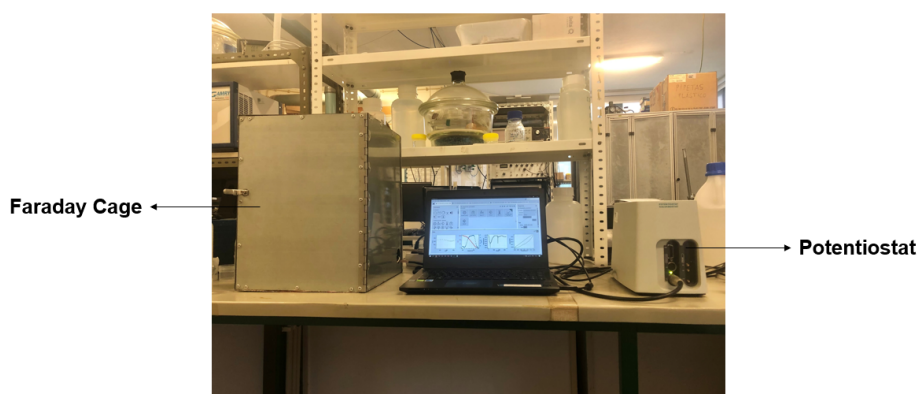
FIGURE 4.11: Setup used for Electrochemical Impedance Spectroscopy using Faraday cage, electrochemical cell (inside Faraday Cage) and potentiostat.

During the measurements of electrochemical impedance, the electrochemical cell was placed inside a Faraday cage (metallic box acting as an electromagnetic shield). It is important to use the faraday cage because the electromagnetic field associated with the current and the voltage extends around the impedance element and can interact with metallic parts or with other currents flowing nearby, making the measured impedance unstable and poorly defined [37].

4.3.3   Scanning Electron Microscopy and Energy Dispersive Spectroscopy

In order to study the morphology of the copper samples after electrochemical experiments, SEM/EDS was carried out. SEM images of the samples after potentiodynamic polarization were then obtained in order to confirm the presence of pits in copper samples. Sample preparation and SEM/EDS analysis were carried out at the Materials Centre of University of Porto (CEMUP), at the Imaging, Microstructure and Microanalysis Unit Laboratory (IMICROS). Images were taken with different magnifications, namely: 20 000x, 25 000x and 50 000x. The energy of the electron beam used was 15 keV and the surface morphology of the samples was evaluated with the secondary electron detector (SE).

4.4   Chemical analysis of the water used in the functional tests

In order to assess the influence of the water used in the functional test on the problem under study, chemical analysis of the water used in the functional tests were requested and analysed. The analysis was carried out by the Hidrax laboratory. The following chemical parameters were analysed: pH, total hardness, chlorine, chloride, bicarbonate and sulfate. The request for analysis of these parameters is related to the values found in the literature that correlate the appearance of pitting with the physicalchemical parameters of the water [8, 24, 26].

Chapter 5

Results and Discussion

In this chapter, the results of the three distinct phases of experimental work are presented and discussed. Firstly, the results of identification and examination of pits presented in heat exchangers are presented. Secondly, the results of the metallographic characterization of the different samples from different heat exchangers are presented. In the third phase, the polarization curves and Nyquist/Bode Diagrams obtained through potentiodynamic polarization and electrochemical impedance spectroscopy are analysed.

5.1 Identification and examination of pits

In this subchapter, the results of the analysis of the pits identified in the copper coils of heat exchangers that were in operation are described. Initially, the results of the analysis of the corrosion products observed on the external surface of the heat exchanger through X-ray diffraction spectra will be presented, followed by the results of the analysis of the pits present on the internal surface of the coils using scanning electron microscopy/ energy dispersive spectroscopy.

Figure 5.1 A) shows an image of stereoscopic magnifier of the external section of heat exchanger and corresponding XRD Spectra.
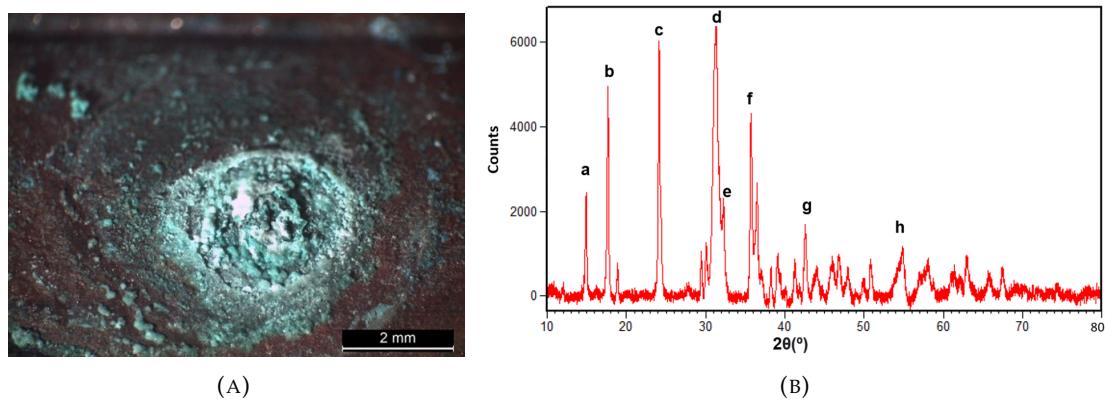
FIGURE 5.1: (A) Image of stereoscopic magnifier of corrosion products present on the external surface of heat exchanger (pit of section identified as D3). (B) The XRD spectra of green layer present on the external surface of heat exchanger corresponding to malachite $(Cu_2CO_3(OH)_2)$

.

Figure 5.1 A) reveals the presence of corrosion products with green color in the external surface of the heat exchanger. The corrosion products present in the external section of heat exchanger are compact and uniform in the region of pit . According to Lyte the presence of corrosion products can help to stop continued growth of pits and prevent major water leaks [30]. The XRD spectra of the green layer in figure 5.1 B) presents peaks corresponding to malachite $(Cu_2CO_3(OH)_2)$. Table 5.1 shows in the first column the peaks identified by the analysis software (that have the highest intensity), second column shows 2θ values and in the third column values of d corresponding to the distance between lattice planes for the given diffraction peak that we calculate using Bragg's law. In the fourth column are the miller indices, indices were obtained based on the conversion table of the HighScore Plus software, since the crystal structure is monoclinic.

TABLE 5.1: Corresponding parameters of XRD spectra extracted from figure 5.1

peak	$2\theta(°)$	$\theta(°)$	$d = \lambda/2sin(\theta)(\text{Å})$	(hkl)
a	14.81	7.41	5.98	020
b	17.52	8.76	5.06	021
c	24.10	12.05	3.69	022
d	31.32	15.66	2.85	-102
e	32.26	18.13	2.77	-112
f	35.58	17.79	2.52	042
g	42.38	21.19	2.13	052
h	54.84	27.42	1.67	-125

Formation of malachite $((Cu_2CO_3(OH)_2)$ is associated with the following chemical equation [43]:

$$2Cu^{2+} + CO_3^{2-} + 2OH^- \longrightarrow Cu_2CO_3(OH)_2 \tag{5.1}$$
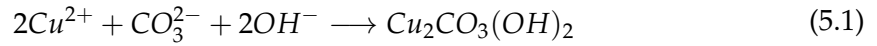
Typically, the formation of malachite (a copper carbonate hydroxide) is associated with environments rich in carbonate (CO_3^{2-}), as can be seen in the equation above, which checks the presence of this ion in the water circulating inside the heat exchanger. Malachite is a copper carbonate and has been associated with the formation of pitting corrosion in the inner surface of copper pipes [28, 44], the presence of malachite on the external surface of the heat exchanger reveals that after pit initiation, the corrosion products that typically are present on the inner surface of the coil collapse for external section the heat exchanger.

Next, different samples with pitting corrosion extracted from the internal section of the heat exchanger described in the experimental section were characterized morphologically using SEM and chemically using the EDS. The internal section of the heat exchanger was analysed to verify the morphology of the pits and the corrosion products.
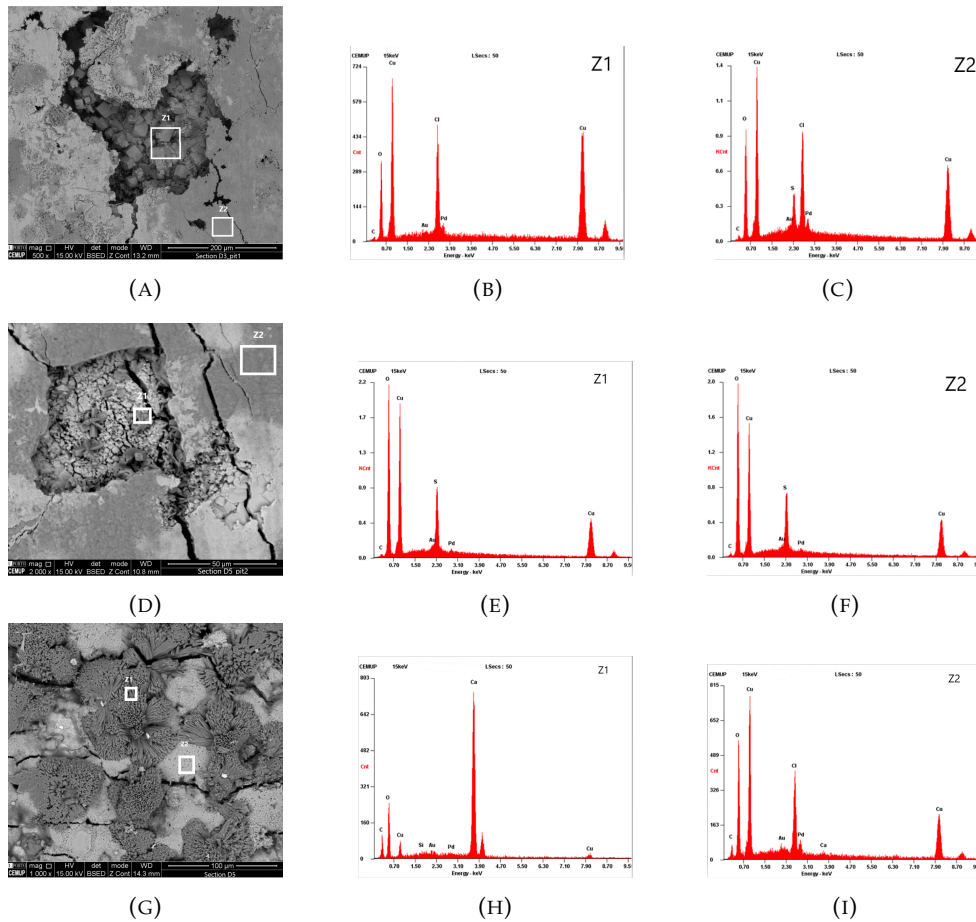
FIGURE 5.2: (A) SEM micrograph showing the region with pit from section D3 (cold water coil). (B) EDS spectra at the surface of pit. (Z1) confirming the presence of chlorine. (C) EDS spectra at the surface of pit (Z1) alongside pit. (D) SEM micrograph showing the region with pit from section D5 (hot water coil). (G) SEM micrograph showing the region without pit from section D5 (hot water coil).

.

Figure 5.2 A) shows a pit with irregular geometry and small micro-pits in the circulating area. The image in Backscattered electrons (BSED) shows the presence of perfect copper oxide crystals (Cu_2O) with a cubic structure inside the pit. The EDS spectra shows significant amounts of Oxygen (O), Copper(Cu) and Chlorine (Cl) inside the pit (region Z1) and Chlorine (Cl) and Sulfur(S) concentrated alongside the pit (region Z2). According to the semi-quantitative analysis, significant amounts of Chorine (Cl) is notable in pit compared to the uncorroded area highlighting its influence on copper pitting corrosion. The morphology of the pit and corrosion products found to support the type of pit found and addressed previously in the state-of-the-art review, classified as pitting type I.

In the pit illustrated by figure 5.2 B) in Backscattered electrons (BSED) with corrosion products with distinct morphology inside the pit. The EDS spectra reveals the presence of

Oxygen (O), Copper(Cu) and Sulfur (S) in the regions inside (Z1) and outside of pit (Z2).

In picture 5.2 C) the presence of pitting corrosion is not observed. Semi-quantitative analysis reveals the presence of Oxygen (O), Copper (Cu), Carbon (C), Calcium (Ca) and Chlorine (Cl). The calcium revealed by the spectra may be due to calcium carbonate, being associated with carbonation of calcium carbonate, which is mostly found in harder water. Water circulating in the coils naturally contains calcium carbonate, taking into consideration that calcium carbonate at high temperatures decomposes forming a protective layer [45].

In summary, morphological differences were observed in the shape of different pits. In the case of cold water coil the value of the area of the pit is higher compared to hot water coil. EDS analysis revealed distinct corrosion products in coils that circulated cold water and hot water, the semi-quantitative analysis revealed mostly the presence of elements such as Chlorine (Cl) inside the pit in cold water coil. On the other hand, the EDS analysis reveals the presence of Sulfur (S) inside pit in hot water coil.

5.2   Metallographic characterization

This subchapter presents in figure 5.3 metallographic characterization of different copper samples that were studied during this work obtained by optical microscopy.
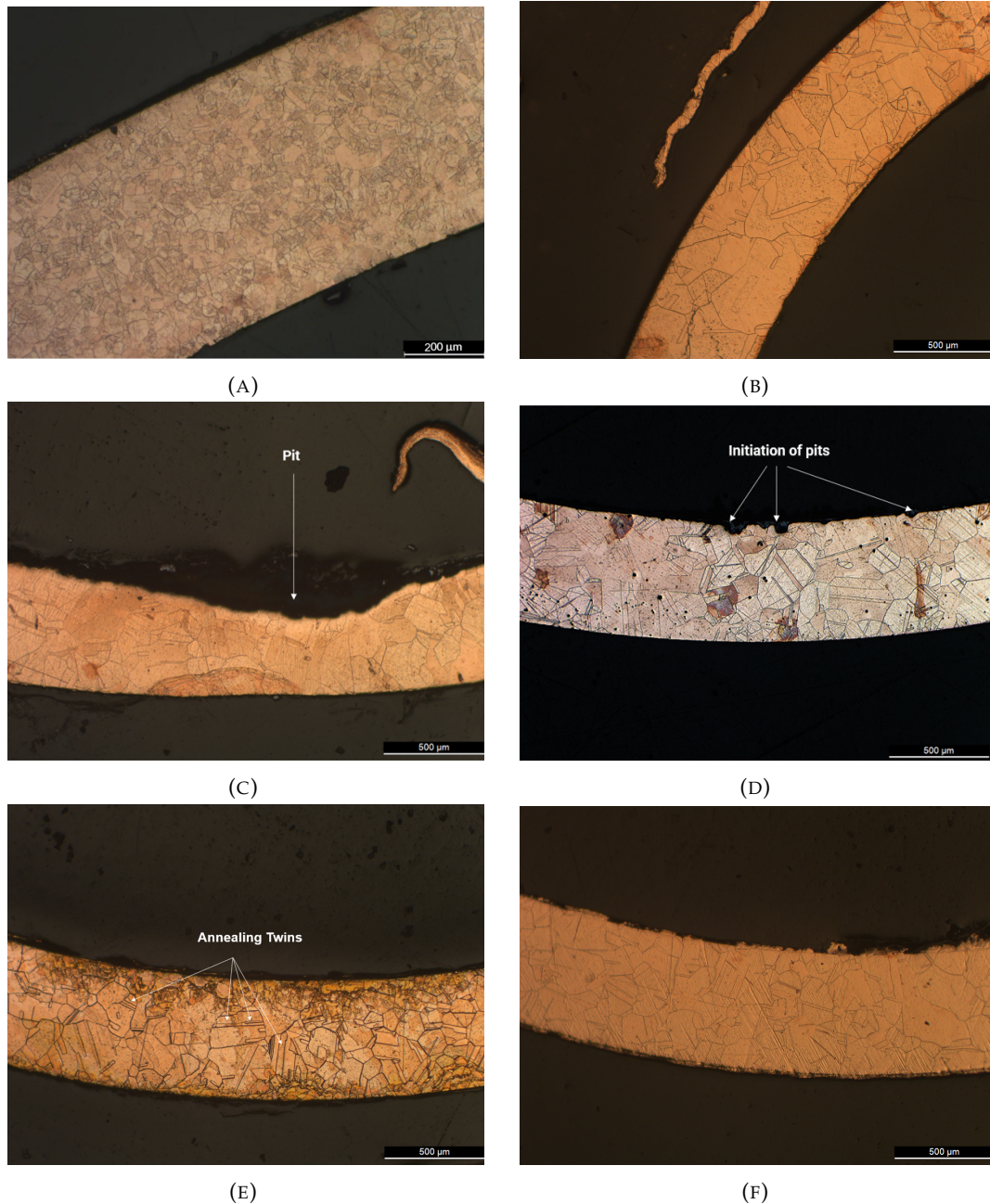
FIGURE 5.3:   Microstructure of Sample (A) Cu_Raw Material (before oven inlet) (B) Cu_Furnace Brazing (after oven outlet) (C) Cu_Operation_pit1 (region of pit)(D) Cu_Operation_pit2 (region of pit initiation) (E) Cu_Operation _without pit1(region without pit) (F) Cu_Operation _without pit2 (region without pit).

One of the most important aspects in metallographic analysis concerns grain boundaries, so famous in metallurgy, which can be classified as crystallographic discontinuities/ structural disorder within materials that serve as boundaries in the region separating two differently oriented crystals [46].

Figure 5.3 A) shows the microstructure of the sample identified as Sample Cu_Raw Material obtained by optical microscopy. Analysing the figure 5.3 A), the grain boundaries can be clearly observed, being dense, compact and homogeneous. Can be observed the presence of equiaxed grains recrystallized throughout the region, evenly distributed. The microstructure was already observed in the literature by Bagherian [47].

Figure 5.3 B) shows the microstructure of sample Cu_Furnace Brazing. There is an increase in grain size compared to sample Cu_Raw Material, as expected. The increase in grain size is due to the fact that the sample was exposed to heat treatment in furnace brazing process and considering that grain boundaries are regions with high energy, with favorable energy conditions (in this case temperature) the microstructure will evolve in the direction of energy minimization, decreasing grain boundaries and increasing grain [46].

Figure 5.3 C) shows the microstructure of sample Cu_Operation_pit1. Analysing the figure is verified the presence of pitting initiation with "wide" geometry, according to the classification given by the ASTM standard presented in the state-of-the-art review [10]. According to Gentil, the grain boundary works as an anodic area in relation to the grain (cathodic area), hence the preferential attack at the grain boundaries is an electrochemical phenomenon [9].

Figure 5.3 D) shows the microstructure of sample Cu_Operation_pit2. The figure shows the initiation of two pits simultaneously with "wide" geometry. In the microstructure are observed small black holes distributed along the central area of the sample. Marzena explains the appearance of small holes due to non-metallic inclusions in the material. According to the author corrosion attack can be initiated in the area of non-metallic inclusions rich in phosphorus in the pipe material mainly inside the copper grains, but locally also along its borders [48]. The grain size heterogeneity in the sample's different areas is highlighted.

Figure 5.3 E) presents the microstructure of sample E, it is possible to analyse the grain boundaries with clarity, verifying the existence of polygonal grains and "annealing twins" inside the grains. Annealing twins are formed a recovery mechanism for materials

that have low stacking energy. Typically, the formation of annealing twins is associated with metals with a Face Centered Cubic (FCC) structure, such as copper (Cu) and nickel (Ni) [46].

The figure 5.3 F) shows the microstructure of sample Cu_Operation _without pit2, the grain appears to be more homogeneous compared with samples of figures C and D. The grain size area was determined in the Image J software. The results were compared through the statistical representation. The histograms referring to the grain area of the different samples are represented in the figure 5.4 and were set up by counting the area of grains.

(A)

(B)

(C)

(D)
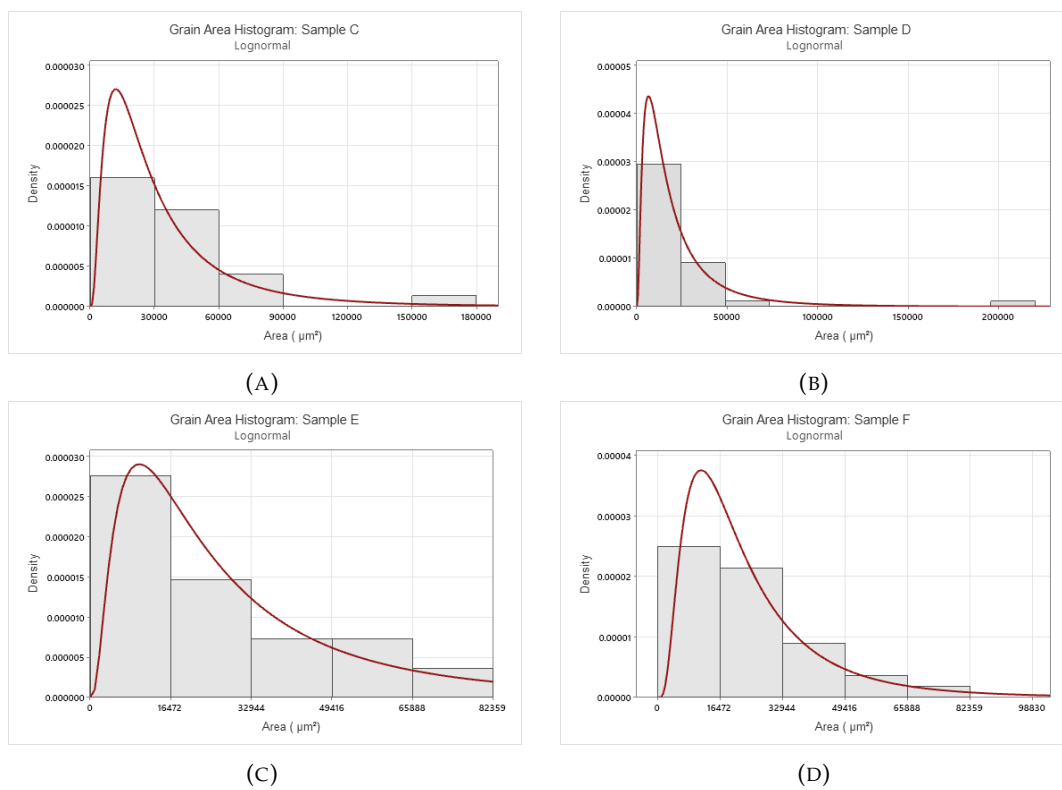
FIGURE 5.4: Grain Area Histogram of Sample (A) Sample C (B) Sample D (C) Sample E D) Sample F

The histograms obtained were then fitted by a log-normal distribution. The heterogeneity of the grain area is higher in samples of figures C and D comparing to samples of figures E and F.

5.3   Analysis of Polarization Curves

In this subchapter, the experimental results of the electrochemical experiments are presented, having as the main goal to obtain polarization curves that allowed to analyse the electrochemical behavior of different samples in different environments. The figures 5.5-5.6 illustrates the graphical representation of polarization curves resulting from the electrochemical tests in different environments for different samples (Cu_Raw Material, Cu_Lubsec AL7 and Cu_Furnace Brazing). Polarization curves are represented in potential as a function of current density in logarithmic scale. The applied potential was measured in relation to the reference electrode of Silver/Silver Choride (Ag/AgCl).
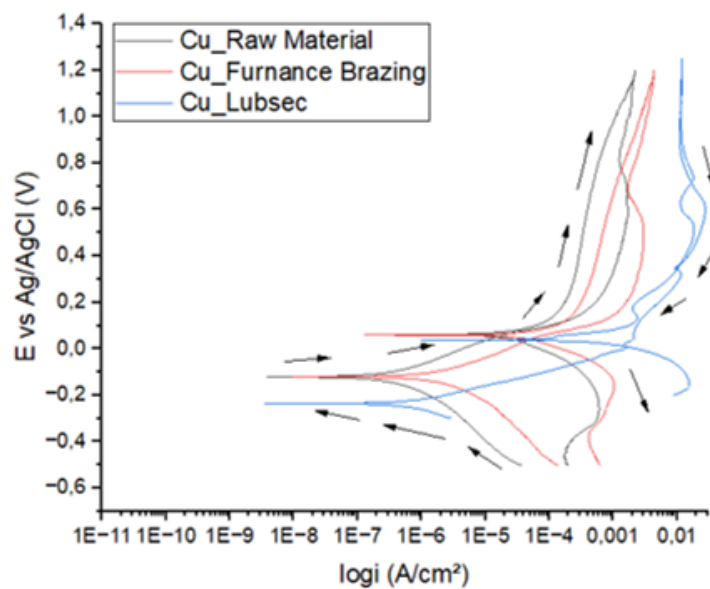
FIGURE 5.5:   Graphic representation of polarization curve for sodium chloride (NaCl). for different samples: Cu_Raw Material, Cu_Lubsec and Cu_Furnace Brazing.
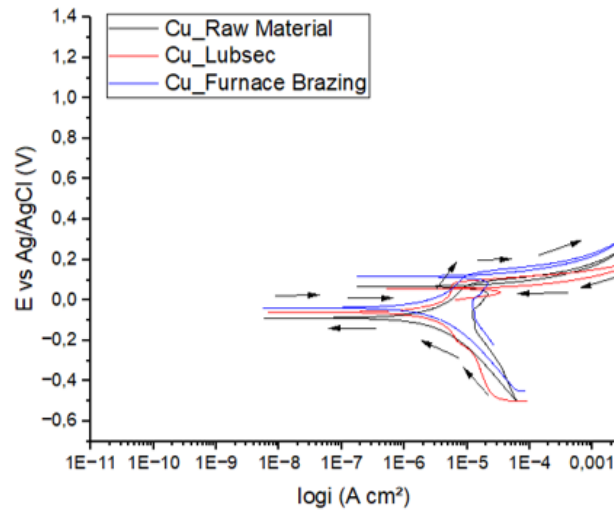
FIGURE 5.6: Graphic representation of polarization curve for 0.1 M of sodium sulfate (Na_2SO_4) for different samples: Cu_Raw Material, Cu_Lubsec and Cu_Furnace Brazing.

Potentiodynamic polarization allows interpretation of the polarization curves and inference about the occurrence of pitting corrosion through the analysis of electrochemical parameters such as the pitting potential (E_{pit}) and the repassivation potential (E_{rp}). The electrochemical parameters extracted from figures 5.6 - 5.6 are listed in table 5.2. The table shows the corrosion potential E_{corr}, the pitting potential, E_{pit} and the repassivation potential E_{rp}.

TABLE 5.2: Corresponding electrochemical parameters extracted from figures 5.6 - 5.6

Test solution	Sample	E_{corr}(v)	$E_{pit}(V)$	$E_{rp}(V)$
0.6 M NaCl	Cu_Raw Material	-0.121	-	-
	Cu_Furnace Brazing	-0.121	-	-
	Cu_Lubsec	- 0.201	-	-
0.1 M Na_2SO_4	Cu_Raw Material	-0.150	0.073	0.063
	Cu_Furnace Brazing	-0.125	0.088	0.071
	Cu_Lubsec	- 0.130	0.090	0.067

The difference of behaviour for each test solution is visible. In the case of test solution of 0.6 M of NaCl where the chloride (Cl^-) concentration is considerably high, polarization curve doesn´t showed passivation region and Pitting Potential (E_{pit}). It can be observed that both curves presented a similar evolution for the different types of samples. In both cases, the curves presented a negative hysteresis curve, showing no signs of localized corrosion. The cathodic reaction of copper in 0.6M of sodium chloride (NaCl) solution is well known to be the oxygen reduction and follows the following chemical reaction: $O_2 + H_2O + 4e^- \longrightarrow 4OH^-$ [49]. On the other hand, in anodic region the lower applied potential extending to a peak current density due to the dissolution of copper into Cu^+, a region of decreasing current is reached due to the formation of CuCl and a region of suddenly increase due to soluble $CuCl_2^-$ [49]. The reaction process is reported to be diffusion controlled with no evidence of a protective oxide layer. The corrosion potential for samples corresponding to the raw material and which underwent the furnace brazing process is the same, indicating a similar resistance to uniform corrosion. On the other hand, the sample with Lubsec showed a more negative corrosion potential, indicating a lower resistance to uniform corrosion.

For test solution with 0.1 M of sodium sulfate where the sulfate concentration is considerably higher, the polarization curve shows a region of passivation and pitting potential. Analysing the graph of figure 5.6 at the initial period of anodic polarization is observed a narrow region corresponding to the passivation region, where the passivation region is defined when it is verified that over a given potential range, the corrosion current density remains constant. The passivation region started at potentials from approximately 0 to 0.2V. According to the literature the narrow region observed is caused by the adsorption of chemical species $Cu(SO_4^{2-})$ and $Cu(OH)^-$ [19].

In all samples the pitting potential is more positive than the repassivation potential, indicating the occurrence of pitting at the electrode surface and the increase in current density may be associated with the initiation of pitting. After experiments was made a surface inspection of the samples in 0.1M of sodium sulfate in order to confirm the initiation of pits by scanning electron microscopy, whose images are represented in figure 5.7.

(A)   (B)   (C)
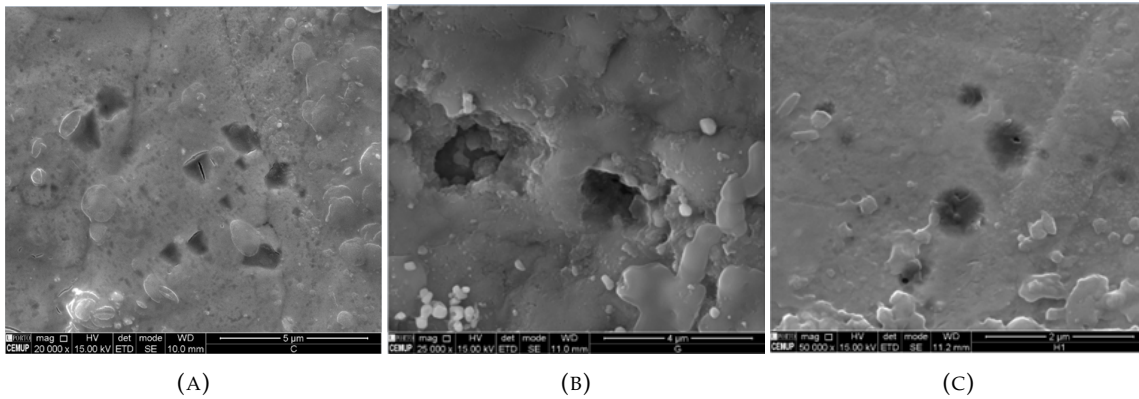
FIGURE 5.7: Copper samples after electrochemical experiments corresponding to (A)
Cu_Raw Material. (B) Cu_Furnace Brazing. (C) Cu_Lubsec.

Through the analysis of the figure above, the sample Cu_Furnace Brazing is the sample with the largest pit diameter. It can also be seen that the sample with Lubsec presents dark spots on the surface, the chemical composition in the darker spots was analysed by EDS. Figure 5.9 shows different regions of the surface of the copper sample with Lubsec after electrochemical experiments.
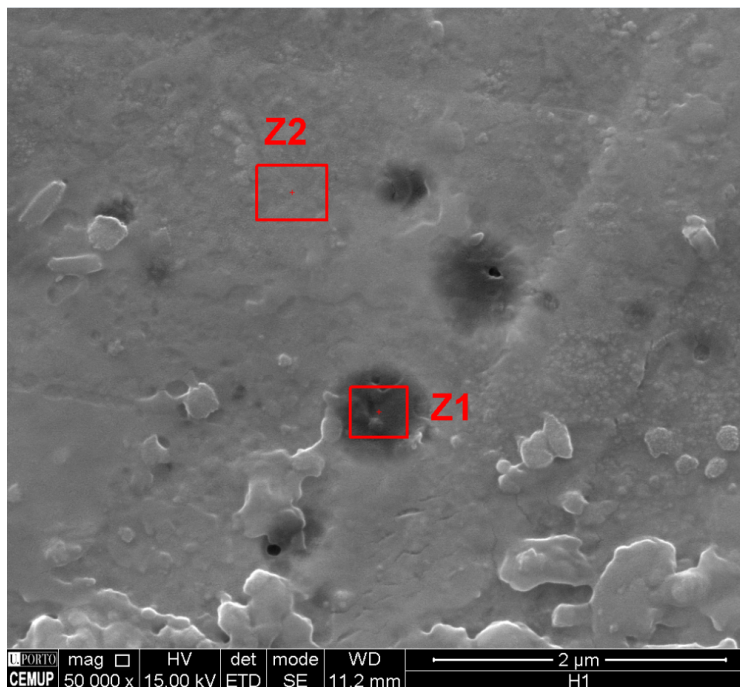
FIGURE 5.8: SEM micrograph corresponding to copper sample with 1 mL of Lubsec
showing several pits.
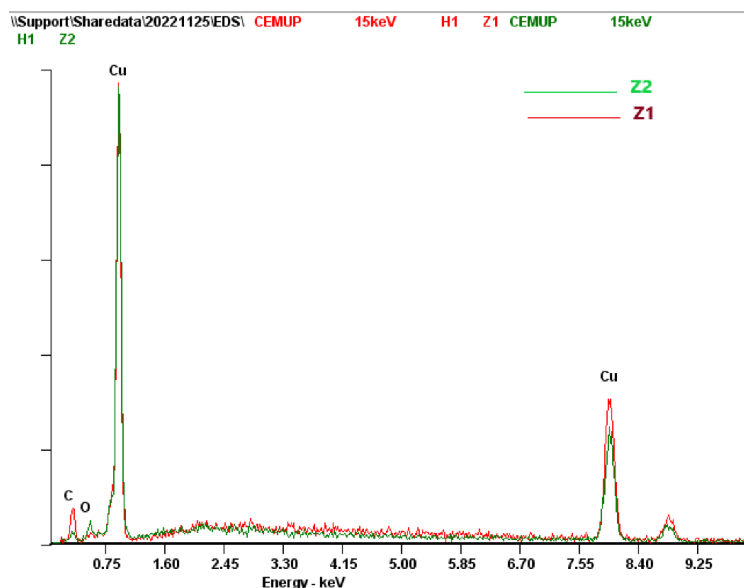
FIGURE 5.9: EDS spectra showing a higher amount of carbon in region Z1 (location of pit initiation) in comparison with region Z2 (region without pit).

Analysing the SEM image of the figure 5.8 in secondary electron mode it is possible to verify the presence of dark spots in the region of pitting corrosion, which we designated as Z1 and in the lighter area, without pitting, we designated as Z2. The image below demonstrates the existence of 4 pits with different geometries and diameters. It is also shown the SEM analysis of the area with and without pits on the surface of the analysed sample. The presence of several spots along the sample may be related to the non-uniform application of the Lubsec on the sample surface and consequently the appearance of darker spots in preferential regions. Lubsec has in chemical composition hydrocarbons, hence the EDS spectra for an energy of 15 Kev reveals the presence of carbon. Carbon is cited in the literature by several authors as one of the main factors responsible for the initiation of pitting [9, 20, 21]. It is therefore concluded that in a test solution containing sodium sulfate, Lubsec oil is an enhancer of pitting corrosion in copper (Cu-DHP).

5.4   Analysis of Nyquist and Bode Diagrams

In this subchapter, the EIS diagrams are presented in figures 5.10 A) and B) for the different copper samples (Cu _Raw material, Cu _Lubsec and Cu _Furnace Brazing) and for different immersion times, namely 1h and 168h in a solution 0.6 M of sodium chloride (NaCl).

FIGURE 5.10:   (A) Graphic representation of Nyquist Diagram for 0.6M of sodium chloride (NaCl).   (B) Graphic representation of Bode Diagram for 0.6M of sodium chloride (NaCl).

The Nyquist diagram for the different samples in solution of 0.6 M of sodium chloride (NaCl) shows two semicircles for all sets of samples. It is important to note that one of the semicircles is due to the double electrical layer and the charge transfer resistance and the other that begins to be drawn at low frequencies is associated with a diffusion transport process. The sample designated by Cu _Raw Material with an immersion time of 1h is the sample that shows the highest diameter value for high frequencies. It is noted that with the increase of the immersion time it can be seen that the distance between the semicircles decreases, this behaviour can be explained by the formation of corrosion products in the surface of copper with time as will be explained.

In the Bode diagram, with the graphical representation corresponding to $|Z|$ vs frequency is highlighted a resistive behaviour for high frequencies, followed by a capacitive behaviour (10^3 to 10^0 Hz) and followed by a resistive behaviour which becomes well defined for an increase of immersion time (168h). Complementary, in the Bode diagram with the graphical representation of phase angle as a function of frequency are observed two and three-time constants, through the phase angle peaks in the Bode diagram. One of the time constants can be associated with the copper oxide layer and another one with the charge transference. At high frequencies, the samples showed values near 0° and a constant value, corresponding to the electrolyte resistance.

Through qualitative analysis was verified that the different copper samples have more significant variations with 1h of exposure than with 168h of exposure in the test solution of sodium chloride (NaCl).

Then, the EIS diagrams are presented in figures 5.11 A) and B) for the different copper samples (Cu _Raw material, Cu_Lubsec and Cu_Furnace brazing) and for different immersion times, namely 1h and 168h immersed in a solution 0.1 M of sodium sulfate (Na_2SO_4).
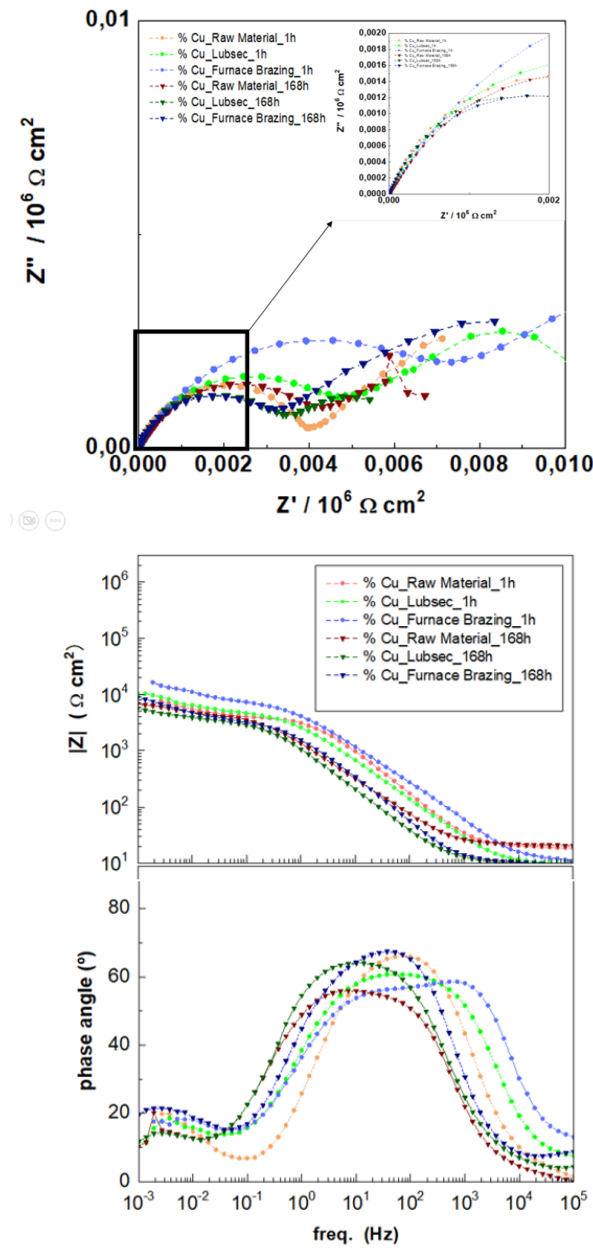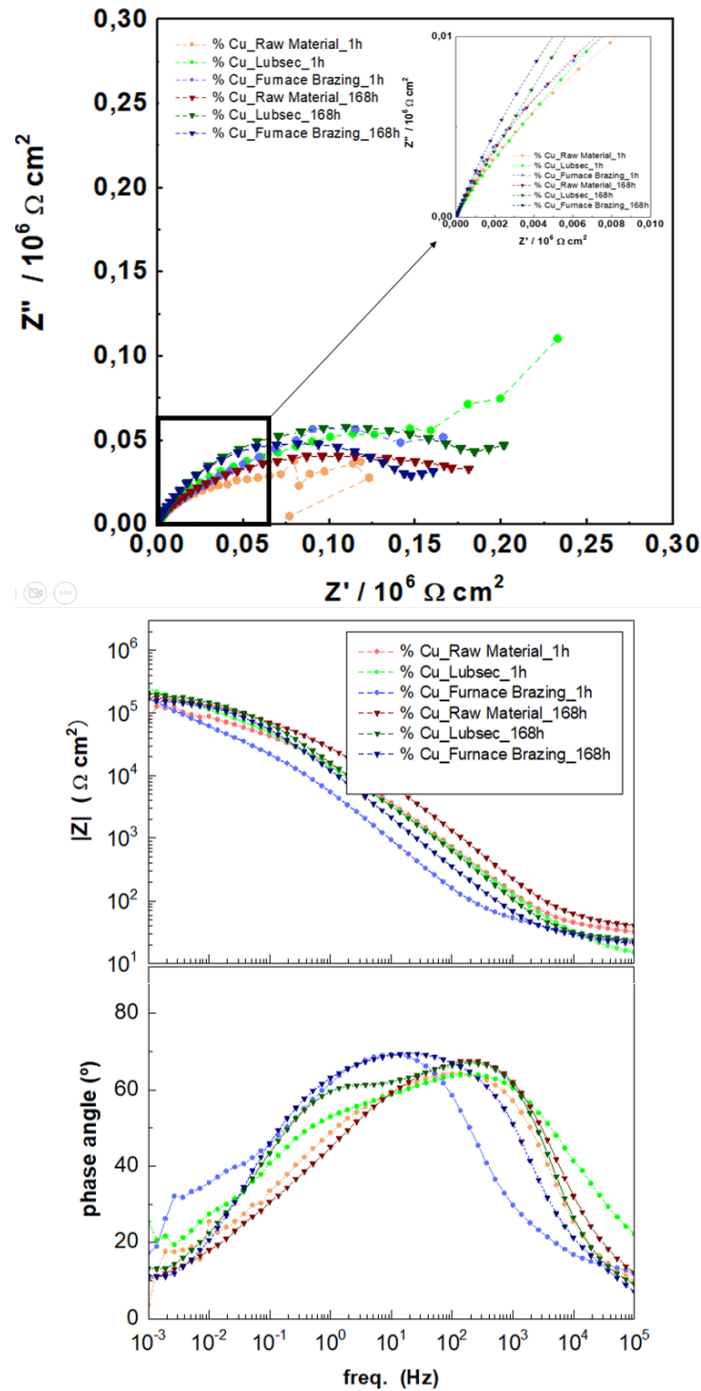

FIGURE 5.11: (A) Graphic representation of Nyquist Diagram for 0.1M of sodium sulfate (Na_2SO_4). (B) Graphic representation of Bode Diagram for 0.1M of sodium sulfate (Na_2SO_4).

Similarly to the sodium chloride (NaCl) solution, the Nyquist diagram for the different samples in sodium sulfate (Na_2SO_4) solution shows two semicircles for all sets of samples. The sample corresponding to furnace brazing was the sample with the highest diameter value for high frequencies, indicating greater corrosion resistance. With increasing immersion time (168h) the diagrams showed a slight increase in impedance, which may be related to the development of a film of corrosion products.

In the Bode diagram, with the graphical representation corresponding to $|Z|$ vs frequency is highlighted a resistive behaviour for high frequencies, followed by a capacitive behaviour (10^4 to 10^{-1} Hz). Complementary, in the Bode diagram with the graphical representation of phase angle as a function of frequency are observed two time constants, through the peaks in the Bode diagram. One of the time constants can be associated with the oxide layer and the other with charge transfer resistance. At high frequencies, the samples presented values close to $0°$ and a constant $|Z|$ value, corresponding to the electrolyte resistance.

For a better interpretation of the electrochemical behaviour through the EIS technique, it is necessary to use an equivalent circuit to describe the electrochemical behaviour of copper samples in a solution of NaCl and Na_2SO_4 and estimate the different corrosion parameters. Figure 5.12 shows the electric circuits used to fit experimental data in which Rs is the electrolyte resistance, R1 is associated with the pore resistance (resistance of the solution present in the pores) and CPE1 (constant phase element) corresponds to the capacitance of the layer of passive and/or surface products and/or corrosion. CPE2 and R2 are associated with the region of surface corresponding to the active metal. The Warburg element (W_0) was used in order to describe diffusion and to achieve a correct adjustment to the experimental results.

(A)

(B)
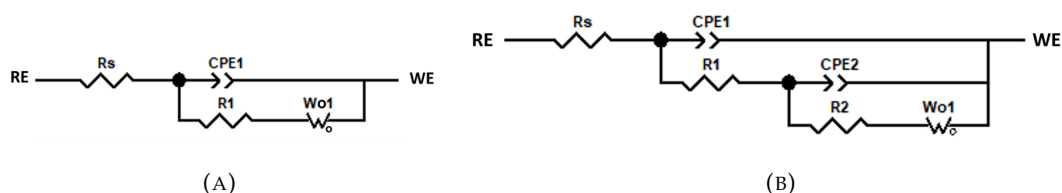
FIGURE 5.12: (A) Electric circuit used to fit experimental data in NaCl solution. (B) Electric circuit used to fit experimental data in NaCl and Na_2SO_4 solution.

The experimental results were fitted using ZView software and are represented in table 5.3. The quality of the fitting was evaluated by the value of χ^2 that resulted in all cases less than 10^{-3}, indicating a good fit.

TABLE 5.3: Parameters obtained by fitting the EIS results to the equivalent circuits

| Test solution	Sample	R_s (Ω cm^{-2})	CPE_1 (F cm^{-2} s^{n-1})	n_1	R_1 (Ω cm^{-2})	CPE_2 (F cm^{-2} s^{n-1})	n_2	R_2 (Ω cm^{-2})
0.6 M NaCl (1h)	Cu_Raw Material	18.58	3.05×10^{-5}	0.821	3798	-	-	-
	Cu_Furnace Brazing	10.68	1.58×10^{-5}	0.801	447.5	3.48×10^{-5}	0.630	7643
	Cu_Lubsec	8.98	6.76×10^{-5}	0.731	5044	-	-	-
0.6 M NaCl (168h)	Cu_Raw Material	21.44	6.65×10^{-5}	0.830	305.3	1.06×10^{-4}	0.698	3978
	Cu_Furnace Brazing	-	-	-	-	-	-	-
	Cu_Lubsec	9.37	1.19×10^{-4}	0.772	3595	-	-	-
0.1 M Na_2SO_4 (1h)	Cu_Raw Material	32.32	9.41×10^{-6}	0.771	4737	1.80×10^{-5}	0.351	185600
	Cu_Furnace Brazing	13.09	4.70×10^{-6}	0.771	3913	4.96×10^{-5}	0.479	433270
	Cu_Lubsec	12.73	1.45×10^{-5}	0.720	11605	1.45×10^{-5}	0.208	78120
0.1 M Na_2SO_4 (168h)	Cu_Raw Material	39.55	4.56×10^{-6}	0.790	18662	1.29×10^{-5}	0.494	199110
	Cu_Furnace Brazing	22.43	1.88×10^{-5}	0.777	101160	5.23×10^{-5}	0.765	47004
	Cu_Lubsec	23.83	7.75×10^{-6}	0.919	4499	9.82×10^{-6}	0.613	177270

Analsing the results of the table 5.3 it is verified a small difference in the values of the solution resistance (R_s) represented in the third column. This oscillation of values may be related to the variation of the distance between the working electrode and the counter electrode during the experimental activity. Typically in more conductive solutions the distance between electrodes is not so relevant, hence the oscillations of values are lower in the case of NaCl solution compared to the Na_2SO_4 solution [50]. The discrepancy of values associated with Rs does not compromise the quality of the remaining analysis experimental results.

Comparing the CPE1 values presented in the fourth column for the NaCl solution, which are associated with the oxide layer on the surface and which reflect the non-ideal dielectric properties, it was observed that the copper sample designated by Cu_furnace brazing presented lower values, showing that the oxide film in this system has better protective properties and indicating higher corrosion resistance, as previously stated through the Nyquist diagram. With the increase of the immersion time, the CPE value for the three types of samples increased. This increase may be related to the formation of corrosion products over 168h on the copper surface as can be seen in figure 5.13. There is a difference in the corrosion products formed on the surface of the different samples. In the case of the sample corresponding to the raw material the corrosion products are uniform along the surface. On the other hand, the sample with lubsec and that has undergone the oven demonstrate not to be uniform. In the case of 1h of immersion the n values are between 0.731 and 0.821 and in the case of 168h immersion are between 0.772 and 0.830.
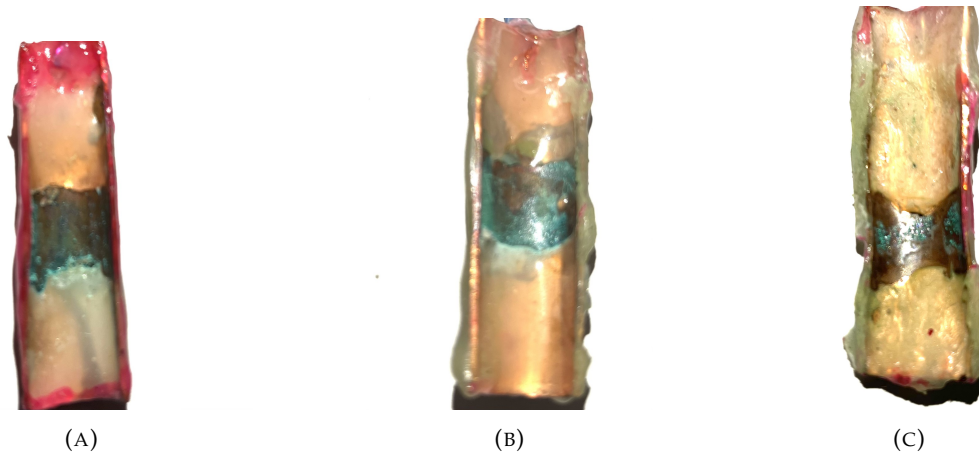
FIGURE 5.13: Copper samples after 168h of immersion in solution of 0.6M NaCl corresponding to Cu_Raw Material (B) Cu_Lubsec (C) Cu_Furnace Brazing

Analysing the values of R_1 for the NaCl solution it can be seen that it´s higher in the case of the sample designated as Cu_Furnace Brazing compared with the other samples, which may indicate higher quality of the film present on the surface, as explained previously. It is known that for values of total system resistance higher or equal to 10^6 Ωcm^2, indicate the formation of an oxide film in the passive state. The values of R obtained are lower than 10^6 Ωcm^2, indicating that the surface is in the active state, that is, it has an unstable oxide film. In the case of NaCl solution, the order of magnitude is around 10^3 Ωcm^2 indicating the formation of an unstable film, not being verified the formation of a film called "passive film", being in agreement with the results obtained in the polarization, given that the polarization curves do not present the formation of the passivation region.

In the case of the Na_2SO_4 solution it is verified that the CPE1 values for 1h of immersion are higher in the sample designated Cu_Lubsec, showing that the oxide film in this system has worse protective properties.In the case of 1h immersion, the n values are between 0.721 and 0.771 and in the case of 168h immersion, they are between 0.707 and 0.919, indicating values close to 1 and consequently the response of a non-ideal capacitor for longer immersion times.

It was noted that the resistance values of the samples in a solution of Na_2SO_4 are considerably high compared to NaCl solution, which corresponds to the presence of a passive film, being in agreement with the results obtained in polarization for a solution of Na_2SO_4. It is important to emphasise that the impedance in NaCl solution is about 10 times lower than in Na_2SO_4.

5.5   Analysis of chemical parameters of water used in functional tests

The following figures show the pH and chlorine concentration values of the recirculated water currently used for carrying out the functional tests over the 11 months of 2021 according to the values provided by Bosch.
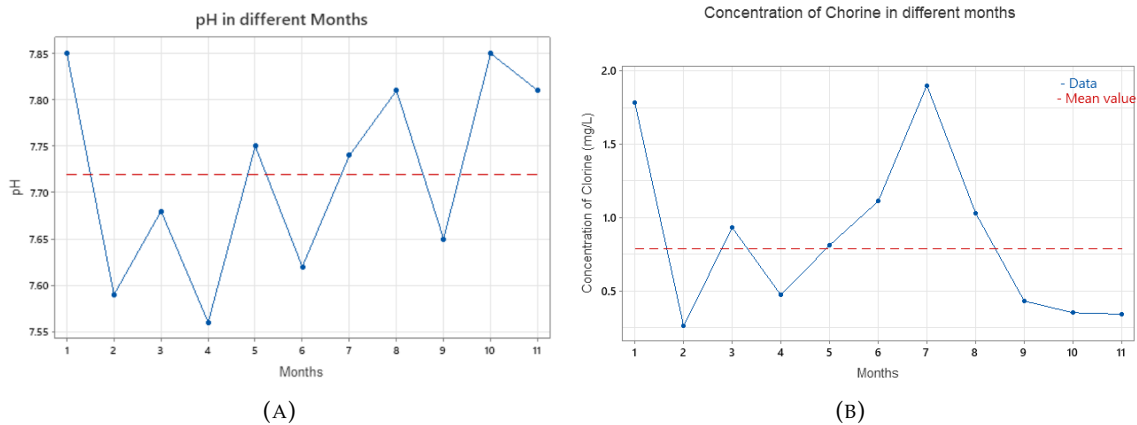
FIGURE 5.14:   (A) Analysis of pH of water used in functional tests. (B) Analysis of free chloride (Cl_2) concentration of water used in functional tests.

Analyzing figure 5.14 we see that the average is pH = (7.72 ± 0.09). The average free chlorine value over 2021 was approximately (0.79 ± 0.38) mg/L. After comparing the concentration of free chlorine with the values presented in the literature it is verified that the value is considerably higher [26]. Considering that purge time is reduced, water droplets can remain inside the heat exchanger in the period between the packing of the equipment and its delivery to the customer. Table 5.4 shows the results of the chemical parameters of the recirculated water currently used for carrying out the functional tests corresponding to the month of July 2022.

TABLE 5.4: Chemical parameters of the recirculated water currently used for carrying out functional test.

Parameter	Value	Unit
pH	8.03	
Chlorine (Cl_2)	1.22	mg/L
Chloride (Cl^-)	105	mg/L
Sulfate (SO_4^{2-})	108	mg/L
Bicarbonate (HCO_3^-)	54	mg/L

Chapter 6

Recommendations to minimize Failures

After an analysis of the manufacturing process of the heat exchangers and considering the results of experimental work it is important to make recommendations to minimize the probability of failure caused by pitting corrosion. The recommendations for the manufacturing process are the following:

1) Introduce a process step to wash the copper coils before the furnace brazing process to avoid carbon residues from Lubsec on the internal surface of coils during flare formation.

2) Use filters in order to remove excess of chlorine present in the water used in the functional tests. The main goal is to prevent the presence of water droplets remaining in the heat exchangers during the period before the installation of the appliance, because the presence of water droplets may act as a catalyst.

Chapter 7

Conclusions and Future Work

This chapter presents the conclusions of the present work and the recommendations for the continuity of the study of pitting corrosion in copper heat exchangers.

7.1 Conclusions

The present work studied root causes of pitting corrosion in copper heat exchangers manufactured in the production section of Bosch Thermotechnology, S.A - Aveiro. Pitting Corrosion in copper heat exchangers has a high number of variables involved, making this problem very complex. Regarding the difficulties for the development of this work, the data collection was a difficult part of the study considering that the lack and quality of certain data on the exact location where field failures occurred were the main barriers found in carrying out a quality statistical analysis.

The manufacturing process of the heat exchangers used in gas water heaters was analysed. After a detailed analysis of the manufacturing process of the heat exchangers, some of the following stages were considered more critical namely: application of Lubsec, furnace brazing and water used in the functional tests.

The pits were analysed with x-ray diffraction and SEM/EDS. The x-ray diffraction revealed the presence of malachite on the outside of the heat exchanger and the SEM/EDS analysis revealed the presence of majorly chlorine in the cold water coil and sulphur in the hot water coil.

In order to reproduce the different transformations that copper undergoes during the manufacturing process, was elaborated an experimental plan for the preparation of copper samples to reproduce the real conditions of the manufacturing process and were

used different experimental techniques to study their influence, namely: potentiodynamic polarization and electrochemical impedance spectroscopy. Regarding the experimental work, were used two test solutions with distinct chemical parameters. The sample with 1mL of Lubsec in test solution of 0.1M of sodium sulfate solution (Na_2SO_4), evidenced the initiation of pitting in areas whose EDS spectra revealed higher carbon intensity, being associated with oil Lubsec used in the flare formation.

With this work, were suggested recommendations related to manufacturing process to minimize the failures, at the process level, namely: the washing of the coils so that no traces of oil remain and the use of filters in the water used in the functional tests, taking into account that the chlorine values presented are considerably high.

7.2 Future Work

The complexity and the high number of parameters involved is considerably high. Due to the unavailability of some information and the time needed to complete this work, it is recommended for future work to continue some topics that would be interesting to study.

Firstly, one of the relevant topics would be having enough field data to establish a correlation between the chemical parameters of the water and locations where failures occurred. In this first phase, the water analysis is still determinant, for what we contemplate the analysis of water samples in what concerns pH, hardness and some important anions namely: chlorides and sulfates would be interesting. These data are relevant for the interpretation of the results of the analysis of the equipment in a more sustained way.

It is also suggested to study the influence of the loads present in heat exchangers, namely: water temperature, the influence of pressure variations and water flow in the heat exchanger. The influence of water temperature should be studied using for example module of critical pitting temperature of gamry potentiostat. The influence of pressure variations and water flow can be studied through CFD simulations. These simulations would be interesting to be carried out in CFD in order to establish a correlation between the velocity regime (laminar or turbulent) along the heat exchanger and a greater probability of the removal of the copper oxide layer in critical regions. The last one is an important parameter because fluid velocity may be a factor as it can lead to vortex and remove the copper oxide layer and increase susceptibility to corrosion in certain areas of the heat exchanger.

In order to understand the influence of the functional tests, water could be placed in copper samples and left for a few months in contact with the sample and could be carried out in electrochemical experiments to really understand their influence.

Appendix A

Potentiostat Fundamentals

Commercial potentiostat varies in design according to different brands, but a typical potentiostat requires essentially three component circuit: a control circuit, an electrometer circuit and a current flower in which operational amplifiers are used [51]. Explaining in a simple way the three component circuit: the electrometer circuit represented above measures the potential difference between the working electrode (WE) and reference electrode (RE) using a differential amplifier. The measure of potential difference is fed into the control circuit which applies a current using a counter electrode (CE). Then, the current flowing throught the counter electrode is measured by current follower, which typically takes the form of current to voltage converter, which typical takes the form of current to a voltage (I/E) converter.
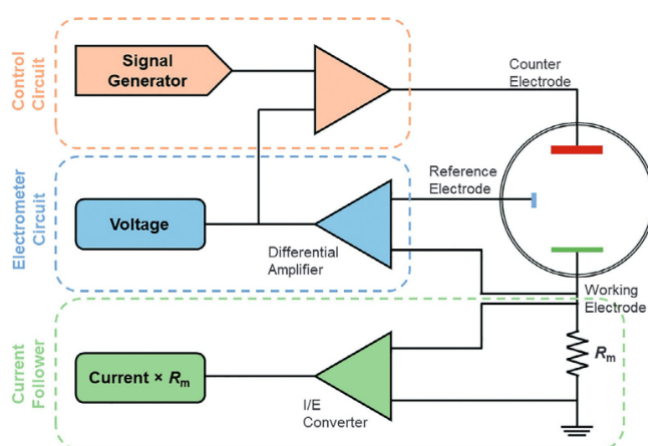

FIGURE A.1: Simplified electric circuit of a typical potentiostat: control circuit, electrometer and a current flower. Adapted from [51].
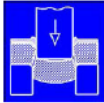
Appendix B

Datasheet of LUBSEC AL7

FICHA TÉCNICA — FUCHS

LUBSEC AL 7

Lubrificante evanescente para trabalhos metálicos.

Descrição

O LUBSEC AL 7 é um lubrificante evanescente que se destina a operações de corte e de embutição/deformação quando queremos evitar as operações posteriores de limpeza e desengorduramento.

O LUBSEC AL 7 é constituído por hidrocarbonetos reforçados com agentes de untuosidade, aditivos anti soldadura e aditivos anti desgaste específicos.

O LUBSEC AL 7 foi especialmente concebido para trabalhos com metais não-ferrosos, no entanto, pode ser igualmente recomendado para trabalhos com outras ligas metálicas.

A velocidade de evaporação de LUBSEC AL 7 é extremamente rápida.

Aplicação

O LUBSEC AL 7 pode ser aplicado por impregnação, por irrigação, gota a gota ou com um sistema de pulverização.

Vantagens / Benefícios

- Inodoro, especialmente durante a sua aplicação.

- Grande poder lubrificante.

- Possui um grande poder de lubrificação assegurando uma boa utilização com uma reduzida quantidade de produto.

- Depois da evaporação do LUBSEC AL 7, o filme residual depositado nas superfícies trabalhadas é negligenciável.

Dados Técnicos

Características	Unidade	Valor	Norma
Aspecto		liquido incolor	VISUAL
Densidade a 15 ℃	g/cm^3	0,76	NF EN ISO 12185
Viscosidade Cinemática a 20 ℃	mm^2/s	1,90	NF EN ISO 3104
Ponto de Inflamação	℃	47	NF EN 22719
Teste em Lâmina de Cobre		1a	NF EN ISO 2160

FIGURE B.1: Datasheet of Lubsec oil showing description, application, benefits and technical data.

Appendix C

Copper Corrosion Products

The Copper Corrosion products detected by X-ray diffraction in corrosion failures described in the literature are summarized in the following table:

TABLE C.1: Copper Corrosion Products described in the literature found by X-ray diffraction. Adapted from [52, 53]

Product of Corrosion	Chemical Formula
cuprite	Cu_2O
tenorite	CuO
malachite	$Cu_2CO_3(OH)_2$
cuprous chloride	CuCl
cupric chloride	$CuCl_2$
atachamite	$Cu_2Cl(OH)_3$
antlerite	$Cu_3SO_4(OH)_4$
brochantite	$Cu_4SO_4(OH)_6$
posnjakite	$Cu_4(OH)_6SO_4H_2O$
langite	$Cu_4(OH)_6SO_42H_2O$

Appendix D

Dimensions of electrochemical cell

During the project, were drawn technical drawings in STL (Standard Triangle Language) in order to design the electrochemical cell to carry out the electrochemical experiments in the same conditions (distance between electrodes). Dimensions of sample holder and upper region of the electrochemical cell are represented in the figure D.1 B) and C):

| (A) | (B) | (C) |
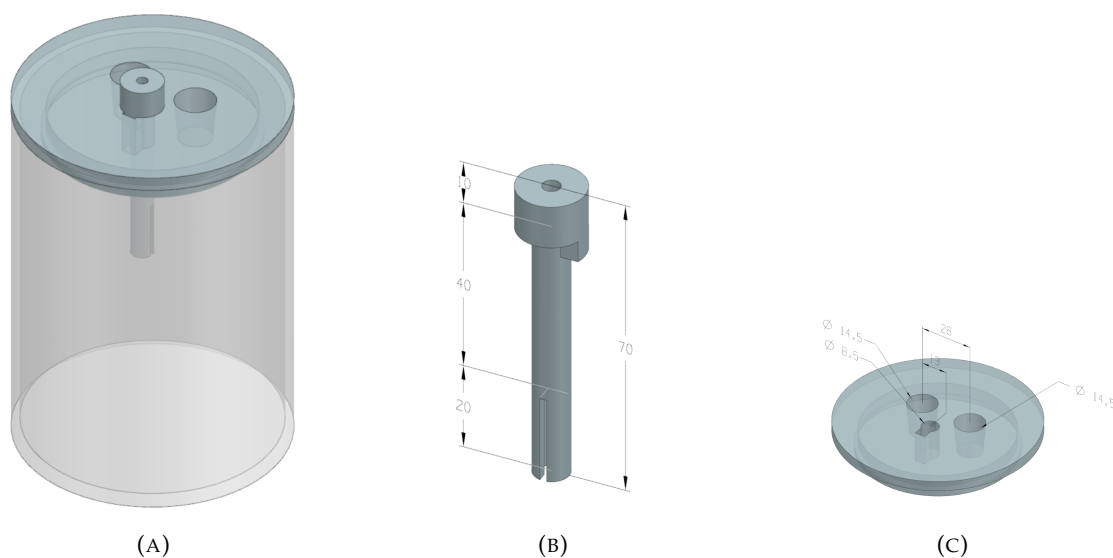
FIGURE D.1: (A) Electrochemical cell. (B) Dimensions of sample holder. (C) Dimensions of the upper region of the electrochemical cell.

A Stratasys dimension elite 3D Printer represented in the figure D.2 was used to print the electrochemical cell and printing was carried out at Bosch Thermotechnology, S.A - Aveiro.

FIGURE D.2: The 3D printer Stratasys dimension elite used to design the morphology of the electrochemical cell, whose operations is based on FDM (Fused Deposition Modeling) technology. The impression material used was ABS P340 amorphous polymer (Stratasys).

Bibliography

[1] E. Bowman, N. Thompson, D. Gl, O. Moghissi, M. Gould, and J. Payer, "International measures of Prevention, Application, and Economics of Corrosion Technologies Study," *NACE international*, vol. 216, pp. 2–3, 2016. [Cited on page 1.]

[2] G. T. Burstein, C. Liu, R. M. Souto, and S. P. Vines, "Origins of pitting corrosion," *Corrosion Engineering Science and Technology*, vol. 39, pp. 25–30, 2004. [Cited on page 1.]

[3] Y. Tan, "Understanding the effects of electrode inhomogeneity and electrochemical heterogeneity on pitting corrosion initiation on bare electrode surfaces," *Corrosion Science*, vol. 53, no. 5, pp. 1845–1864, 2011.

[4] K. R. Tarantseva, "Models and methods of forecasting pitting corrosion," *Protection of Metals and Physical Chemistry of Surfaces*, vol. 46, no. 1, pp. 139–147, 2010. [Cited on pages 1 and 13.]

[5] ISO, "Corrosion of metals and alloys –Vocabulary (ISO 8044:2020)," 2020. [Online]. Available: https://www.iso.org/standard/71134.html [Cited on pages 9 and 13.]

[6] M. G. Fontana and N. D. Greene, "Corrosion engineering," *McGraw-Hill*, 1986. [Cited on pages xi, 9, 10, 11, and 13.]

[7] E. McCafferty, "Introduction to corrosion science," *Springer New York*, 2010. [Cited on page 10.]

[8] S. A. Farooq, A. Raina, M. I. Ul Haq, and A. Anand, "Corrosion Behaviour of Engineering Materials: A Review of Mitigation Methodologies for Different Environments," *Journal of The Institution of Engineers*, pp. 1–23, 2022. [Cited on pages xi, 11, 19, and 54.]

[9] V. Gentil, "Corrosão," *LTC*, 1996. [Cited on pages 12, 17, 18, 22, 61, and 67.]

[10] ASTM, "ASTM G46-21 Standard Guide for Examination and Evaluation of Pitting Corrosion," 2021. [Online]. Available: www.astm.org, [Cited on pages xi, 13, and 61.]

[11] Z. Szklarska Smialowska, "Pitting and crevice corrosion," *NACE International*, 2005. [Cited on pages 13 and 16.]

[12] G. Frankel, "Pitting corrosion of metals: a review of the critical factors," *Journal of the Electrochemical society*, vol. 145, no. 6, p. 2186, 1998. [Cited on pages xi and 14.]

[13] E. A. Sarver, "Insights into non-uniform copper and brass corrosion in potable water systems," 2010. [Cited on pages xi and 15.]

[14] H. Cong, H. T. Michels, and J. R. Scully, "Passivity and Pit Stability Behavior of Copper as a Function of Selected Water Chemistry Variables," *Journal of The Electrochemical Society*, vol. 156, no. 1, p. 141, 2009. [Cited on pages 15, 16, 17, and 18.]

[15] G. G. Geesey, P. J. Bremer, W. Fischer, D. Wagner, C. Keevil, J. Walker, A. Chamberlain, and P. Angell, "Unusual types of pitting corrosion of copper tubes in potable water systems," pp. 243–263, 1993. [Cited on pages xi and 16.]

[16] S. Lee, J. Kim, and Y. Koo, "Investigation of pitting corrosion of a copper tube in a heating system," *Engineering Failure Analysis*, vol. 17, no. 6, pp. 1424–1435, 2010. [Cited on page 16.]

[17] J. Gibson and B. Karney, "A 30-year review of copper pitting corrosion and pinhole leaks: Achievements and research gaps," *AWWA Water Science*, vol. 3, no. 2, p. 1221, 2021. [Cited on page 16.]

[18] M. Sakai, "A new type of silica-induced "moundless" pitting corrosion in copper observed in Japan," *Heliyon*, vol. 8, no. 8, p. 10110, 2022. [Cited on page 16.]

[19] Y. Ma, X. Tian, J. Yin, J. Chen, and J. Jiang, "The pitting corrosion behavior of copper with different grain size," *International Journal of Electrochemical Science*, vol. 14, no. 5, pp. 4047–4056, 2019. [Cited on pages 17, 22, and 65.]

[20] H. Campbell, "Pitting corrosion in copper water pipes caused by films of carbonaceous material produced during manufacture," *J. Inst Metals*, p. 345, 1950. [Cited on pages 17, 18, and 67.]

[21] T. Iyasu, M. Kuratani, I. Ikeda, N. Tanaka, Y. Yamada, and O. Sakurada, "A Study of Water Treatment Chemical Effects on Type I" Pitting Corrosion of Copper Tubes," *Materials Sciences and Applications*, vol. 11, no. 07, 2020. [Cited on pages 17, 18, and 67.]

[22] S. Reiber, "Corrosion Assessment of Copper Tubing from Residences in the Cobb County-Marietta Water Authority (CCMWA) Service Area," pp. 5–32, 2013. [Cited on pages 17 and 18.]

[23] J. Myers and A. Cohen, "Copper tube corrosion in domestic water systems," *HPAC Engineering*, vol. 77, no. 6, pp. 22–31, 2005. [Cited on pages 17 and 18.]

[24] E. Stansbury and R. Buchanan, "Fundamentals of electrochemical corrosion," *ASM International*, 2000. [Cited on pages 17, 18, and 54.]

[25] A. Warraky, H. Shayeb, and E. Sherif, "Pitting corrosion of copper in chloride solutions," *Anti-Corrosion Methods and Materials*, vol. 51, pp. 52–61, 2004. [Cited on page 17.]

[26] E. Sarver and M. Edwards, "Inhibition of copper pitting corrosion in aggressive potable waters," *International Journal of Corrosion*, vol. 2012, 2012. [Cited on pages 17, 19, 54, and 74.]

[27] J.-P. Duthil, G. Mankowski, and A. Giusti, "The synergetic effect of chloride and sulphate on pitting corrosion of copper," *Corrosion Science*, vol. 38, no. 10, pp. 1839–1849, 1996. [Cited on pages 17 and 18.]

[28] T. Burleigh, C. Gierke, N. Fredj, and P. Boston, "Copper tube pitting in santa fe municipal water caused by microbial induced corrosion," *Materials*, vol. 7, no. 6, pp. 4321–4334, 2014. [Cited on pages xi, 17, 19, 20, and 57.]

[29] S. Roy, J. Coyne, J. Novak, and M. Edwards, "Flow-induced failure mechanisms of copper pipe in potable water systems," *Corrosion Reviews*, vol. 36, no. 5, pp. 449–481, 2018. [Cited on pages xi, 17, 20, and 21.]

[30] D. Lytle and M. Schock, "An investigation of copper pitting corrosion and pinhole leaks," *American Society of Civil Engineers*, pp. 1–8, 2007. [Cited on pages 18, 19, and 56.]

[31] ASTM, "ASTM G61-86 Standard Test Method for Conducting Cyclic Potentiodynamic Polarization Measurements for Localized Corrosion Susceptibility of Iron, Nickel or Cobalt-Based Alloys ," 2018. [Online]. Available: www.astm.org, [Cited on page 22.]

[32] I. Obot, I. Onyeachu, A. Zeino, and S. Umoren, "Electrochemical noise (EN) technique: review of recent practical applications to corrosion electrochemistry research," vol. 33, no. 13, pp. 1453–1496, 2019. [Cited on page 22.]

[33] C. Nyby, X. Guo, J. Saal, S. Chien, A. Gerard, H. Ke, T. Li, P. Lu, C. Oberdorfer, S. Sahu, S. Li, C. Taylor, W. Windl, J. Scully, and G. Frankel, "Electrochemical metrics for corrosion resistant alloys," *Scientific data*, vol. 8, no. 1, p. 58, 2021. [Cited on pages xi and 24.]

[34] W. Choi, H. Shin, J. Man, J. Choi, and W. Yoon, "Modeling and applications of electrochemical impedance spectroscopy (eis) for lithium-ion batteries," *Journal of electrochemical science and technology*, vol. 11, pp. 1–13, 2020. [Cited on pages xi, xv, 25, and 26.]

[35] G. Instrumens, "Basics of Eletrochemical Impedance Spectroscopy," *G. Instruments, Complex impedance in Corrosion*, pp. 1–30, 2007. [Online]. Available: www.gamry.com [Cited on pages xv and 26.]

[36] A. Bastos, "Comportamento Anticorrosivo de Tintas de Base aquosa aplicadas em substratos ferrosos : Estudos por espetroscopia de impedância eletroquimica," 1999. [Cited on pages xi, 27, and 28.]

[37] L. Vadim, "Impedance Spectroscopy: Applications to electrochemical and dielectric phenomena," 2012. [Cited on pages 28 and 53.]

[38] "Bosch Norm N28 Copper, oxygen-free with limited high residual phosphorus content." [Cited on page 31.]

[39] Bosch, "Bosch-Norm N28 CW0024 S001 Copper, oxygen-free with limited high residual phosphorus content ." [Cited on pages xv and 32.]

[40] CEMUP, "Imagem do microscópio eletrónico de varrimento do CEMUP/IMICROS." [Cited on pages xii and 44.]

[41] Struers, "Metallographic preparation of copper and copper alloys." [Cited on page 47.]

[42] "Designation: G61 86 Standard Test Method for Conducting Cyclic Potentiodynamic Polarization Measurements for Localized Corrosion Susceptibility of Iron-, Nickel-, or Cobalt-Based Alloys 1." [Online]. Available: www.astm.org, [Cited on pages 49 and 52.]

[43] S. Suh, Y. Suh, H. Yoon, J. Oh, Y. Kim, K. Jung, and H. Kwon, "Analysis of pitting corrosion failure of copper tubes in an apartment fire sprinkler system," *Engineering Failure Analysis*, vol. 64, pp. 111–125, 6 2016. [Cited on page 57.]

[44] A. House, "A Review of Current Knowledge: Causes of Copper Corrosion in Plumbing systems," pp. 5–22, 2003. [Online]. Available: www.fwr.org [Cited on page 57.]

[45] S. D. Cramer, B. S. Covino Jr, C. Moosbrugger, B. R. Sanders, G. J. Anton, N. Hrivnak, J. Kinson, C. Polakowski, K. Muldoon, S. D. Henry *et al.*, "Asm handbook," *ASM international Materials Park, Ohio*, vol. 13, 2003. [Cited on page 59.]

[46] W. Callister and D. Rethwisch, "Materials science and engineering: an introduction," *Wiley New York*, vol. 9, 2018. [Cited on pages 61 and 62.]

[47] E. Bagherian, C. Bell, M. Cooper, Y. Fan, B. Frame, and M. Rose, "Analysis and quantification of grain size of various DHP copper tubes manufacturing processes," vol. 856, pp. 241–245, 2014. [Cited on page 61.]

[48] M. Lachowicz, "A metallographic case study of formicary corrosion in heat exchanger copper tubes," *Engineering Failure Analysis*, vol. 111, 2020. [Cited on page 61.]

[49] S. Yadav and Y. Archana, "Inhibition of corrosion of copper by substituted triazoles in 3.5 % nacl solution," *J. Chem. Pharm. Res*, vol. 3, pp. 576–583, 2011. [Cited on page 65.]

[50] C. Manole, C. Pirvu, A. Stoian, D. Calderon, Joseand Stanciu, and I. Demetrescu, "The electrochemical stability in nacl solution of nanotubes and nanochannels elaborated on a new ti-20zr-5ta-2ag alloy," *Journal of Nanomaterials*, vol. 2015, 2015. [Cited on page 72.]

[51] A. J. Wain and E. J. Dickinson, "Nanoscale characteristics of electrochemical systems," vol. 18, pp. 1–48, 2021. [Cited on pages xiii and 81.]

[52] I. Vargas, D. Fischer, M. Alsina, J. Pavissich, P. Pablo, and G. Pizarro, "Copper corrosion and biocorrosion events in premise plumbing," *Materials*, vol. 10, no. 9, 2017. [Cited on pages xv and 85.]

[53] D. Lytle and M. Schock, "Pitting corrosion of copper in waters with high pH and low alkalinity," *American Water Works Association*, vol. 100, no. 3, 2008. [Cited on pages xv and 85.]